Chandra News

Issue 20
Spring 2013

Published by the Chandra X-ray Center (CXC)

The Secret X-ray Lives of Planetary Nebulae

Rodolfo Montez Jr. & Joel H. Kastner

Credit: X-ray: NASA/CXC/RIT/J.Kastner et al.; Optical: NASA/STScI

Contents

The *Chandra* Newsletter appears once a year and is edited by Paul J. Green, with editorial assistance and layout by Evan Tingle. We welcome contributions from readers.

Comments on the newsletter, or corrections and additions to the hardcopy mailing list should be sent to: chandranews@head.cfa.harvard.edu.

The Secret X-ray Lives of Planetary Nebulae

Rodolfo Montez Jr. & Joel H. Kastner

The generation of a planetary nebula (PN) has long been appreciated as one of the most photogenic steps in the late evolution of 1–8 $M_\odot$ stars — the last, lovely gasps of asymptotic giant branch (AGB) stars on their way to white dwarfism. Planetary nebulae regularly serve as cover art for astronomy and astrophysics textbooks, and they make stunning subjects for *Hubble* Space Telescope imagery[1]. Beyond their aesthetic value, observations of PNe inform and test theories describing fundamental radiative processes, techniques to determine cosmic abundances, and models of stellar nucleosynthesis and the chemical enrichment of the universe.

Naively, one might assume that the X-ray regime would have little to offer to the PN enthusiasts among the astrophysics community – and vice versa. After all, in classical astrophysics textbooks, PNe are presented as near-ideal examples of $\sim 10^4$ K plasmas in uniform Strömgren spheres that are photoionized by central stars with effective temperatures of $\sim 10^5$ K. Surely, such objects shouldn't be luminous X-ray sources.

However, it had been recognized decades ago that the formation of planetary nebulae should result in strong, X-ray-emitting shocks generated during the abrupt transition from tenuous AGB star to high surface gravity white dwarf (e.g., Volk & Kwok 1985; Zhekov & Perinotto 1996). Furthermore, by the late 90's, the varied shapes and complex structures of PNe revealed by HST had made clear that many, or perhaps most, of the progenitors of PNe began their lives in binary systems (see review by Balick & Frank 2002). In these respects, PNe pose severe challenges to even the most sophisticated hydrodynamical simulations of stellar wind interactions, even as they offer tantalizing clues to the rapid, late binary star evolution processes that might result in X-ray binary systems and the occasional progenitor of a Type Ia supernova.

With its powerful combination of high spatial and spectral resolution, the *Chandra* X-ray Observatory is helping to unlock the potential of planetary nebulae in these astrophysically important areas. As we describe in the following, *Chandra* (and, to a lesser extent, *XMM-Newton*) has established that the majority of PNe do, in fact, harbor X-ray sources — yielding a trove of new insights in realms as diverse as heat conduction in astrophysical plasmas and the "spin-up" of binary companions to mass-losing evolved stars.

Diffuse X-ray Emission: Witnessing the Process of PN Shaping

According to the interacting stellar winds model describing the generation of a PN (Kwok et al. 1978), the nebular shell is formed by the interaction of a nascent fast wind from the stellar core (soon to be a white dwarf star) with an older and denser, slow, dusty AGB wind. This collision of winds should form a post-shock region that fills the nebular cavity with a superheated, tenuous gas, or "hot bubble". Indications of the presence of such hot bubbles within PNe had already come from ROSAT and ASCA observations, which revealed that certain objects harbor relatively

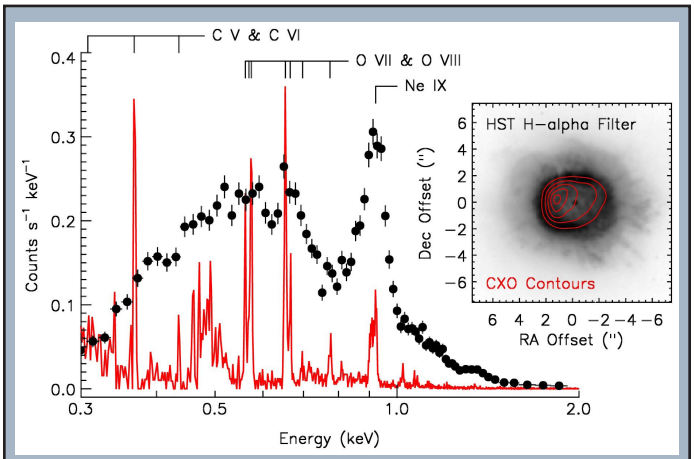

Fig. 1 - The first *Chandra* observations of a planetary nebula were of the compact PN BD +30°3639, and this object has also been the subject of the deepest *Chandra* observations of any PN (a total of ~400 ks in Cycles 1, 6, and 10). Both imaging and gratings (LETG) spectroscopy have been performed, with ACIS-S as the sensor (Kastner et al. 2000; Yu et al. 2009). Shown in the inset are contours of the X-ray-emitting "hot bubble," which fits snugly within the dense nebular rim as imaged by HST in Hα (greyscale). Strong Ne emission from the bubble was already apparent in the ACIS-S3 CCD spectrum (black circles). The LETGS data (red) further reveal that the low-energy end of the hot bubble spectrum is dominated by emission lines of C and O, and constrain its temperature to lie in the range 1.7–2.9 MK (Yu et al. 2009). The forest of lines near 0.5 keV is likely due to C^{6+} ions from the hot bubble penetrating exterior (cooler) nebular gas before recombining (Nordon et al. 2009).

1 See http://hubblesite.org/gallery/album/nebula/planetary/

hard X-ray sources (e.g., Kreysing et al. 1992; Arnaud et al. 1996; Guerrero et al. 2000) — sources seemingly too hard to emanate from the photosphere of a recently unveiled white dwarf (however, see below!).

It took the unprecedented spatial resolution of *Chandra* to confirm these suspicions, in relatively dramatic fashion. Cycle 1 *Chandra* observations of the PN BD +30°3639 (Kastner et al. 2000; Fig. 1) and NGC 6543 (Chu et al. 2001) confirmed that their X-ray emitting regions were extended (as hinted at in ROSAT observations; Leahy et al. 2000, Guerrero et al. 2000). Moreover, in each case, the region of diffuse X-ray emission, as resolved by *Chandra*, fits neatly within the "cool" (~10^4 K), "classical," photoionized nebula as imaged by the *Hubble* Space Telescope (HST) — just as hot bubbles should. A deep X-ray gratings (*Chandra*/LETG/ACIS-S) observation of BD +30°3639 would later establish (Yu et al. 2009; Fig. 1) that its hot bubble plasma consists of almost pure fast stellar wind. This wind material is highly enriched in helium shell burning products, especially C, O, and Ne (Fig. 1).

However, as an assortment of additional detections of diffuse emission trickled in over subsequent *Chandra* cycles (e.g., Montez et al. 2005), and *XMM-Newton* joined in the hot bubble fun (Guerrero et al. 2002; Gruendl et al. 2006), it became clear that PN hot bubbles just aren't hot enough. That is, simple jump-condition calculations yield expected temperatures of T_X~10^7 K or more within the post-shock regions of the fast (~1000 km s^{-1}) winds of PNe — yet *Chandra* and *XMM-Newton* CCD spectra were consistently yielding T_X~10^6 K (Fig. 1). Explanations for this order-of-magnitude discrepancy (which our colleague Noam Soker has dubbed "the low temperature problem") became almost as numerous as PN hot bubble detections themselves: heat conduction from hot (X-ray) bubble to classical (optical) nebula (Steffen et al. 2008); mixing of nebular and hot bubble gas (Chu et al. 2001); the dominant footprint of an early, "slow" fast wind (Arnaud et al. 1996; Akashi et al. 2006); adiabatic expansion and cooling (Soker & Kastner 2003); and, most recently, the bubble's infiltration by an invading army of heat-sapping "pickup ions" (a model inspired by *in situ* Voyager measurements of the solar wind-ISM interface; Soker et al. 2010).

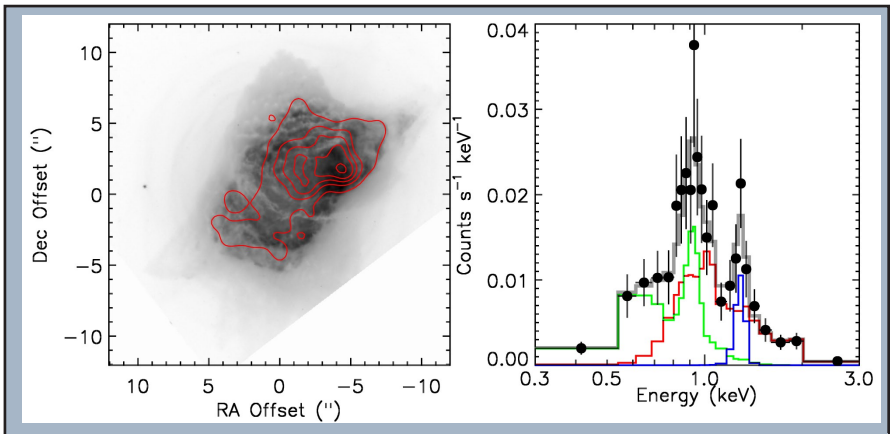

Fig. 2 - *Chandra* and HST observations of the compact PN NGC 7027. Contours of the X-ray emission detected from NGC 7027 (observed for 20 ks in Cycle 1; Kastner et al. 2001) trace the emerging complex structure revealed by the H-alpha HST image (greyscale). The X-ray emission morphology corresponds closely to high-velocity flows that are puncturing the inner shell of the nebula (Cox et al. 2002); the southeast-northwest asymmetry is due to differential absorption across the nebula (Kastner et al. 2001). On the right is the 0.3–3.0 keV spectral energy distribution as extracted from the ACIS-S3 data, indicating the presence of multiple emission features due to the strong shocks in the dense, chemically-enriched, circumstellar environment. In our new spectral analysis (overplotted model), we find a good fit to a two-component thermal plasma (T_X =1 and 8 MK, shown in green and red, respectively) with the addition of an emission line (blue) that is likely due to Mg.

Moreover, by the end of *Chandra*'s first decade it was clear that not all PNe harbor diffuse X-ray-emitting regions and, furthermore, not all diffuse X-ray regions within PNe can be attributed to hot bubbles. Early *Chandra* observations of the famous yet enigmatic PN NGC 7027 had revealed a double-lobed morphology that added new complexity to its already puzzling structure (Kastner et al. 2001; Fig. 2). The diffuse X-ray emission within this PN appears to reveal the process of explosive shrapnel shredding a (more or less elliptical) central bubble. This object is one of only three diffuse X-ray PNe detected thus far that are seen to depart from a classical "hot bubble" morphology: the linear bubble structure that lends the Ant Nebula (Menzel 3) its name appears to be threaded from within by X-ray-emitting jets (Kastner et al. 2003), while a bullet shot out of the core of the S-shaped pre-PN Hen 3-1475 appears to have shocked downstream material to temperatures of a few ×10^6 K (Sahai et al. 2003). Together with the assorted detections and nondetections of hot bubble X-ray emission within PNe obtained by *Chandra* and *XMM-Newton* over their first years of operation (Kastner et al. 2008), these early X-ray de-

tections of collimated flows offered tantalizing hints as to the potential power of X-ray imaging spectroscopy to reveal the shaping processes at work within PNe.

Point Sources at the Central Stars: Just What is Going on Way Down There?

It was recognized early in the *Chandra* mission that, even when imaged at subarcsecond spatial resolution, not all PNe X-ray sources were extended; some objects displayed unresolved sources at their central stars (Chu et al. 2001, Guerrero et al. 2001). While one might expect the Wien tails of the hot "proto white dwarfs" within PNe to produce some X-ray emission, none of the early *Chandra* central star detections were consistent with such an explanation. The central PN point sources were too hard.

The most puzzling example remains that of the Helix Nebula, whose ($\sim 10^7$ K) X-ray emission is far too energetic to originate from a blackbody-like white dwarf photosphere (see image and spectrum on back cover). For old white dwarfs in the field, such hard X-ray emission is typically attributed to coronal emission from a late-type, main-sequence companion (O'Dwyer et al. 2003) — and, in at least some cases, this appears to hold for PN central stars as well (see below). However, attempts to detect such a low-mass companion to the Helix central star have failed thus far, placing severe constraints on the putative companion mass (O'Dwyer et al. 2003).

Serendipitous *Chandra* and *XMM-Newton* observations of another old PN, LoTr 5, revealed an even hotter compact X-ray-emitting source (Montez et al. 2010). However, in this case, there is evidence that the central star has a giant companion that is rotating at near break-up speed (Strassmeier et al. 1997). Attributing the X-ray emission to this companion suggests it resembles members of the class of rapidly rotating giants exemplified by FK Comae, a star that is thought to have emerged from a coalescing binary after a common envelope phase (Jasniewicz et al. 1996). Unfortunately, since the orbit of the central binary within LoTr 5 likely lies nearly in the plane of the sky, we have only limited information concerning its binary system parameters.

Meanwhile, a few candidate post-common envelope (short-period) binaries (PCEBs) are known to reside within PNe (De Marco, Hillwig, & Smith 2008). These PCEBs likely avoided coalescence by unbinding and ejecting their common envelope. During the common envelope phase, an embedded late-type companion accretes angular momentum along with envelope material; such a star should spin up and become more magnetically active (Jefferies & Stevens 1996). Surviving PCEB companions therefore should resemble "born-again" (pre-main sequence) stars, with rejuvenated coronae and (hence) luminous X-ray emission (Soker & Kastner 2002).

To investigate this scenario, we performed a *Chandra* pilot study of two PCEB central stars, and found that both displayed X-ray emission consistent with highly magnetically active companions (Montez et al. 2010). Combined with the serendipitous detection of hard X-rays from the central star within LoTr 5, these results suggested that *Chandra* searches for relatively hard X-ray emission from PN central stars could effectively probe central star binarity. However, it would remain to rule out other potential explanations for relatively hard, point-like emission at PN cores — such as hot circumstellar plasma originating in wind shocks (analogous to those of main-sequence O stars; e.g., Herald & Bianchi 2011), fallback of PN material (perhaps from residual debris disks orbiting the central stars; Su et al. 2007, Bilikova et al. 2012), or sharp departures from local thermal equilibrium (LTE) in the central stars' atmospheres (e.g., Hoogerwerf et al. 2007).

Enter ChanPlaNS

In 2009, a cross-section of the community of PN astronomers gathered in Rochester, NY to develop a comprehensive theoretical and observational campaign aimed at understanding how PNe acquire their diverse array of shapes. Among the conclusions of the resulting "Rochester White Paper" (De Marco et al. 2011) was the need for a systematic *Chandra* survey of PNe — a survey that could yield insights into the X-ray characteristics of PNe far exceeding those already obtained from the small, scattershot sample of PNe assembled during the first decade of *Chandra* and *XMM-Newton*. The PN community rallied around a plan to obtain *Chandra*/ACIS-S3 imaging spectroscopy of a volume-limited sample of PNe — specifically, observations of all ~120 known PNe within ~1.5 kpc of Earth.

This survey (the *Chandra* Planetary Nebula Survey; ChanPlaNS) began in Cycle 12, with a Large

Program consisting of observations of 21 (mostly high-excitation) PNe. The Cycle 12 ChanPlaNS data were combined with archival data for all (14) additional PNe within ~1.5 kpc previously observed by *Chandra* to yield an initial sample of 35 objects, i.e., roughly a quarter of the known PNe within 1.5 kpc. Although data analysis for these 35 PNe is still in its initial stages, PN astronomers now finally have in hand a reasonably healthy sample of observations of representative PNe, and some statistical inferences can already be drawn (Kastner et al. 2012). Specifically, it appears ~70% of PNe harbor some form of X-ray source; ~50% of PNe display X-ray-luminous central stars, while ~30% display soft, diffuse X-ray emission that can be traced to shocks formed by energetic wind collisions. A handful of objects among the initial ChanPlaNS sample of 35 display both varieties of X-ray source (front cover).

Notably, all 10 or so objects among the initial ChanPlaNS sample that show diffuse X-ray emission within hot bubbles have inner shell dynamical ages $\lesssim$5000 yr. It seems, therefore, that the epoch of PN-shaping wind collisions only constitutes the first ~10% of a typical PN's lifetime. These results strongly support other lines of evidence indicating that the varied shapes of PNe are established in the earliest stages of their evolution, perhaps even before the progenitor AGB stars blow away their last, innermost, chemically rich layers of stellar envelope (e.g., Sahai & Trauger 1998).

The fact that so many of the surveyed PNe display relatively hard, point-like X-ray sources at their central stars (Fig. 3) came as a surprise to most of the ChanPlaNS team (with the possible exception of our colleagues You-Hua Chu and Martin Guerrero, who had already recognized the potential significance of such sources). Among the central star X-ray sources, only the core of the famous Dumbbell Nebula (M 27) behaves like the Wien tail of a hot blackbody. These results demonstrate that the (equally famous) Helix Nebula is not exceptional among PNe, in hosting a mysterious, compact source of relatively hard X-rays (see back cover).

A handful of the 21 Cycle 12 targets had been previously observed by *XMM-Newton*, and these objects illustrate how the superior spatial resolution of *Chandra* proves essential in distinguishing diffuse, softer (hot bubble) emission from point-like, harder emission originating with the central stars. The case of NGC 7009 is exemplary in this regard; ChanPlaNS observations of this object, like the earlier observations of the more famous NGC 6543, well illustrate the power of *Chandra* where understanding the origin of PN structure is concerned (Fig. 4).

However, the X-ray emission from even nearby PNe can be extraordinarily faint by, say, supernova remnant standards, and analysis of PN X-ray sources sometimes requires less orthodox strategies. For example, to determine the physical mechanism responsible for the X-ray emission, we consider source photon energy distributions (a method also applied by Getman et al. [2010] to the hundreds of faint sources detected in the *Chandra* Orion Ultradeep Program). Based on this analysis we find that, with the lone exception of the Dumbbell (M 27), the median energies of the compact sources of X-ray emission among the ChanPlaNS sample are incompatible with simple blackbody emis-

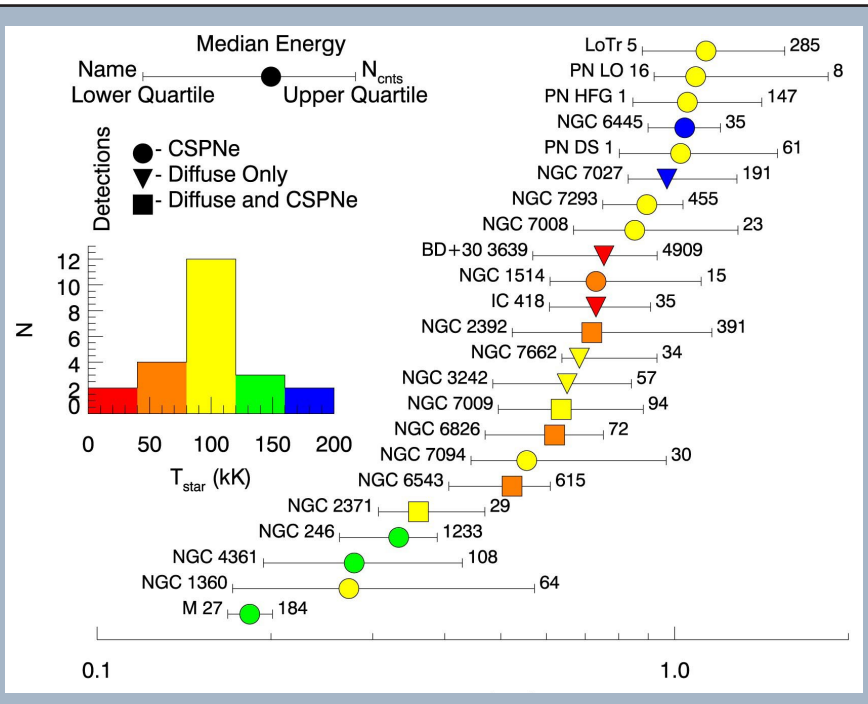

Fig. 3 - Photon energy statistics (net source counts; median energy; first and third quartile energies) for X-ray sources, ordered from lowest to highest median energy (bottom to top). Symbols indicate the nature of each X-ray source (point-like at central star, diffuse, or both central star and diffuse) and are color-coded according to the effective temperature of the central star T_{star} (see inset histogram, which also displays the distribution of T_{eff} for PN central stars detected as X-ray sources). (Figure from Kastner et al. 2012.)

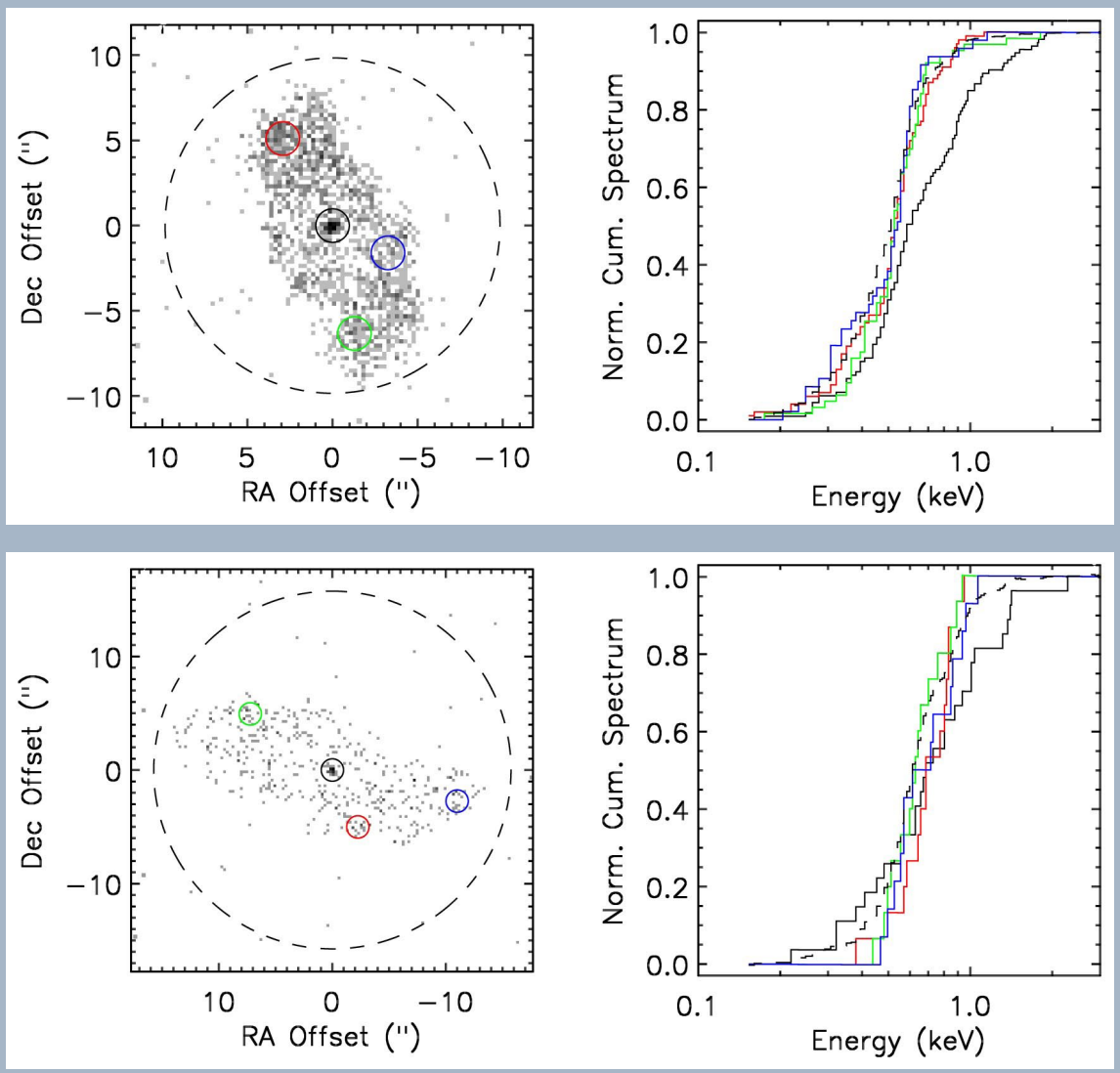

Fig. 4 - Spatial/spectral analysis of *Chandra*/ACIS-S3 imaging spectroscopy of NGC 6543 and 7009 (two of the four nebulae featured on the cover image). The left panels display images of the X-rays detected by *Chandra*, which cleanly distinguishes between diffuse, hot bubble emission and the compact sources at the central stars. In the right panels, we plot the normalized cumulative spectral energy distributions (SEDs) of photons extracted from the regions shown in the left panels; the cumulative SEDs are color-coded (and linestyle-coded) according to their respective spatial extraction regions. These cumulative distributions allow for easy comparison, highlighting differences in X-ray SEDs that are likely due to temperature and/or chemical differences between the diffuse and point-like components. Note, in particular, that (in both cases) the central point source is clearly harder than the hot bubble emission: compare the large-radius extraction region (dashed black), which is dominated by the soft, diffuse emission (note the similarity to the "pure" diffuse emission SEDs shown in red, green, and blue), with the small-radius extraction region centered on the central point source (solid black), which includes relatively little contamination from the diffuse emission.

sion from hot central star photospheres (Fig. 5). Instead, such emission evidently originates, at least in part, from optically-thin thermal plasma emission in the immediate circumstellar environment, although non-LTE atmospheric models for hot PN central stars also predict a significant soft X-ray contribution in certain cases (see below).

Future Prospects

The intial ChanPlaNS results for diffuse and point-like X-ray sources within PNe are pointing out potential new directions in PN research — directions that should be further clarified once results are in for the next batch of (24) ChanPlaNS targets, to be observed during Cycle 14 (Fig. 6). In the case of X-rays from PN central stars, the preliminary ChanPlaNS results — including the fact that ~70% of the sample PNe that are known to harbor binary central stars also display compact, central X-ray sources — point to binary companions as the likely culprits in many if not most cases. Such an origin would lend support to the working hypothesis that most of the known PNe result from binary interactions (De Marco 2009). On the other hand, ROSAT established that most O stars exhibit X-rays, with the emission arising in self-shocking winds. Perhaps ChanPlaNS is establishing that some PN central stars exhibit the very same phenomenon. Indeed, most of the hard X-ray emitting central stars reside on the horizontal part of their H-R diagram evolution, where the wind power, $M\dot{v}^2$, steadily increases until the "turnaround" towards the white dwarf cooling track (Fig. 6). The ChanPlaNS non-detections then tend to increase beyond this turnaround, where the wind power becomes negligible. Detection statistics for Cycle 14 targets in this region of the H-R diagram, combined with further ground-based optical and HST UV spectroscopic investigations of their central stars, should further establish the contribution (or lack thereof) of winds to the central star X-ray budget.

The search for a potential explanation for the relatively hard emission from PN central stars extends beyond ChanPlaNS, in the form of new analyses of X-rays from the central star within K 1–16 and Abell 30 (both of which are just a bit too distant to be included in the ChanPlaNS sample). In our analysis of K 1–16, we invoke non-LTE models of the proto-white dwarf atmosphere, combined with some hot, C-rich circumstellar plasma, to explain the hard X-ray "tail" of the central star (Montez & Kastner 2012, ApJ, in press); in the case of Abell 30, Guerrero et al. (2012) suggest charge exchange or a compact, recently formed hot bubble as potential explanations for its (similar) X-ray spectral energy distribution (SED). The X-ray SEDs of the central stars within these two PNe bear strong similarities to those of a handful of ChanPlaNS sam-

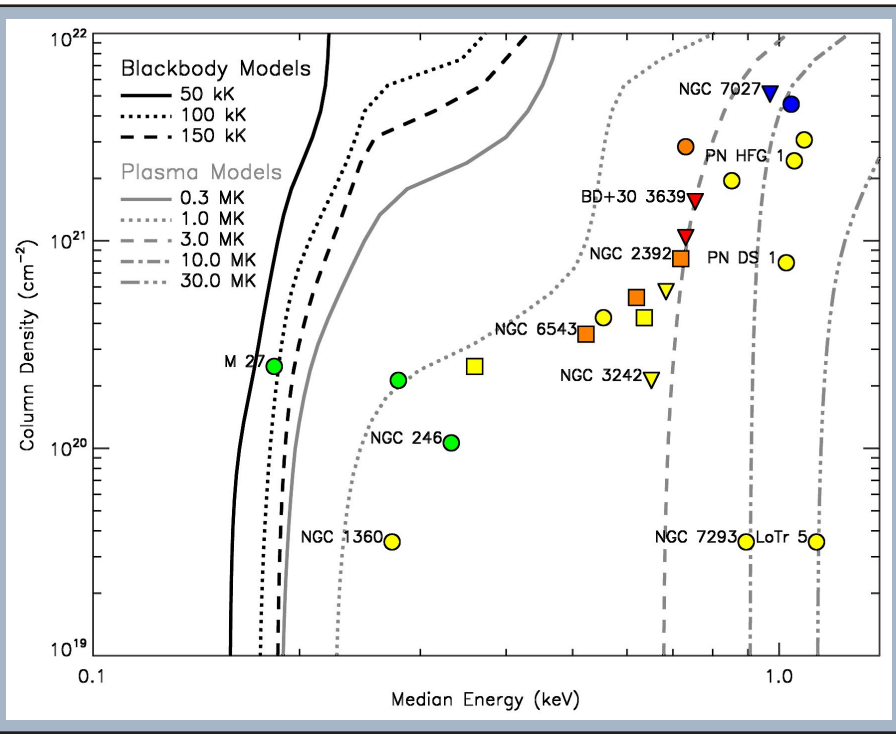

Fig. 5 - Plot of estimated intervening absorbing column density N_H vs. median source photon energy for ChanPlaNS sample PNe detected as either diffuse or point-like X-ray sources (with symbols as in Fig. 3). The N_H estimates are obtained from measurements of the Balmer decrement (Frew 2008). We used a grid of spectral models (absorbed blackbody or absorbed thermal plasma) convolved with the *Chandra*-ACIS-S response to determine model median energies. Clearly, only the central star of the Dumbbell (M 27) can be modeled in terms of simple blackbody emission at temperatures expected of PN central stars; the rest of the central star X-ray sources appear to be affected (in some cases, dominated) by hotter, thermal plasma emission.

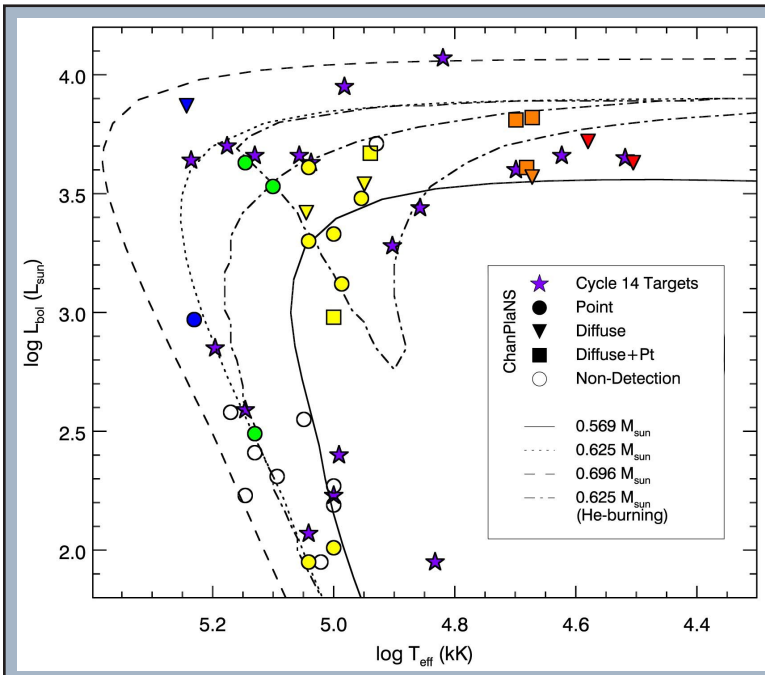

Fig. 6 - HR diagram for central stars of Cycle 12 and archival target PNe, illustrating initial ChanPlaNS results (colored symbols as in Fig. 3 for X-ray detections; nondetections are shown as open circles). The positions of forthcoming (Cycle 14) ChanPlaNS targets are also indicated (as purple stars).

ple objects (NGC 246, 1360, and 4361), suggesting promising new directions for X-ray spectral modeling of these and future ChanPlaNS detections of central stars.

Naturally, it would be beneficial to obtain additional X-ray gratings spectra of additional PN hot bubbles and central stars; BD +30°3639 remains the only PN for which such a gratings study has been published thus far. The Helix and NGC 246 central star X-ray sources are crying out for similar attention. However, most PN X-ray sources are far too faint for gratings observations; even inferences drawn from analysis of the CCD (ACIS) spectra of these objects are likely to be tentative. Still, the growing PN sample size provided by ChanPlaNS affords the opportunity to study an entire class of PNe via, for example, analysis of the composite X-ray spectrum of a set of hot bubbles or central star point sources. In the case of hot bubbles, such investigations should help establish the presence of abundance anomalies of the sort apparent in the gratings spectrum of BD +30°3639 (Yu et al. 2009), thereby shedding light on the as-yet unsolved low temperature hot "bubble" problem. Meanwhile, for central stars, we might be able to tease out differences between abundance patterns and characteristic emission region temperatures for various object classes, thereby distinguishing between the alternative models proposed to explain their hard X-ray "tails."

We hope to obtain *Chandra*/ACIS-S3 observations of the remaining ~60 PNe within ~1.5 kpc in Cycles 15–17, thereby completing a major piece of the multiwavelength observational assault on PNe envisioned in the "Rochester White Paper." Other pieces include (or will include) a parallel *Herschel* Space Telescope Large Program focusing on about a dozen objects selected from among the ChanPlaNS sample PNe ("HerPlaNS"; Ueta et al. 2012), HST Cosmic Origins Spectrograph UV observations of PN central stars, and comprehensive ground-based spectroscopic surveys in the optical & radio, with the Galex and Widefield Infrared Explorer (WISE) all-sky surveys (as well as the *Spitzer* Space Telescope archive; e.g., Bilikova et al. 2012) filling in the picture in the UV and IR, respectively. Hence, astronomers should expect many new, important insights into stellar wind collisions and stellar (binary) evolution from studies of planetary nebulae during *Chandra*'s second decade.

References

[1]Akashi, M., Soker, N., & Behar, E. (2006). MNRAS 368, 1706.
[2]Arnaud, K., Borkowski, K.J., & Harrington, J.P. (1996). ApJ 462, L75.
[3]Balick, B., & Frank, A. (2002). ARA&A 40, 439.
[4]Bilíková, J., Chu, Y. H., Gruendl, R. A., Su, K. Y. L., & De Marco, O. (2012). ApJS 200, 3.
[5]Chu, Y. H., Guerrero, M. A., Gruendl, R. A., Williams, R. M., & Kaler, J. B. (2001). ApJ 553, L69.
[6]Cox, P., Huggins, P. J., Maillard, J. P., et al. (2002). A&A 384, 603.
[7]De Marco, O., Frank, A., Kastner, J., et al. (2011). Asymmetric Planetary Nebulae 5 Conference 19.
[8]De Marco, O. (2009). PASP 121, 316.
[9]De Marco, O., Hillwig, T. C., & Smith, A. J. (2008). AJ 136, 323.
[10]Frew, D. J. (2008). Ph.D. Thesis.
[11]Getman, K. V., Feigelson, E. D., Broos, P. S., Townsley, L. K., & Garmire, G. P. (2010). ApJ 708, 1760.
[12]Gruendl, R. A., Guerrero, M. A., Chu, Y. H., & Williams, R. M. (2006). ApJ 653, 339.
[13]Guerrero, M. A., Chu, Y. H., Gruendl, R. A., & Meixner, M. (2005). A&A 430, L69.
[14]Guerrero, M. A., Gruendl, R. A., & Chu, Y. H.

(2002). A&A 387, L1.
[15]Guerrero, M. A., Ruiz, N., Hamann, W. R., et al. (2012). ApJ 755, 129.
[16]Guerrero, M. A., Chu, Y. H., & Gruendl, R. A. (2000). ApJS 129, 295.
[17]Guerrero, M. A., Chu, Y. H., Gruendl, R. A., Williams, R. M., & Kaler, J. B. (2001). ApJ 553, L55.
[18]Herald, J. E., & Bianchi, L. (2011). MNRAS 417, 2440.
[19]Hoogerwerf, R., Szentgyorgyi, A., Raymond, J., et al. (2007). ApJ 670, 442.
[20]Jasniewicz, G., Thevenin, F., Monier, R., & Skiff, B. A. (1996). A&A 307, 200.
[21]Jeffries, R. D., & Stevens, I. R. (1996). MNRAS 279, 180.
[22]Kastner, J. H., Montez, R., Jr., Balick, B., et al. (2012).AJ 144, 58.
[23]Kastner, J. H., Balick, B., Blackman, E. G., et al. (2003). ApJ 591, L37.
[24]Kastner, J. H., Montez, R., Jr., Balick, B., & De Marco, O. (2008). ApJ 672, 957.
[25]Kastner, J. H., Soker, N., Vrtilek, S. D., & Dgani, R. (2000). ApJ 545, L57.
[26]Kastner, J. H., Vrtilek, S. D., & Soker, N. (2001). ApJ 550, L189.
[27]Kreysing, H. C., Diesch, C., Zweigle, J., et al. (1992). A&A 264, 623.
[28]Kwok, S., Purton, C. R., & Fitzgerald, P. M. (1978). ApJ 219, L125.
[29]Leahy, D. A., Kwok, S., & Yin, D. (2000). ApJ 540, 442.
[30]Montez, R., Jr. & Kastner, J. H., (2012). ApJ in press.
[31]Montez, R., Jr., De Marco, O., Kastner, J. H., & Chu, Y. H. (2010). ApJ 721, 1820.
[32]Montez, R., Jr., Kastner, J. H., De Marco, O., & Soker, N. (2005). ApJ 635, 381.
[33]Nordon, R., Behar, E., Soker, N., Kastner, J. H., & Yu, Y. S. (2009). ApJ 695, 834.
[34]O'Dwyer, I. J., Chu, Y. H., Gruendl, R. A., Guerrero, M. A., & Webbink, R. F. (2003). AJ 125, 2239.
[35]Sahai, R., Kastner, J. H., Frank, A., Morris, M., & Blackman, E. G. (2003). ApJ 599, L87.
[36]Sahai, R., & Trauger, J. T. (1998). AJ 116, 1357.
[37]Soker, N., & Kastner, J. H. (2003). ApJ 583, 368.
[38]Soker, N., & Kastner, J. H. (2002). ApJ 570, 245.
[39]Soker, N., Rahin, R., Behar, E., & Kastner, J. H. (2010). ApJ 725, 1910.
[40]Steffen, M., Schönberner, D., & Warmuth, A. (2008). A&A 489, 173.
[41]Strassmeier, K. G., Hubl, B., & Rice, J. B. (1997). A&A 322, 511.
[42]Su, K. Y. L., Chu, Y. H., Rieke, G. H., et al. (2007). ApJ 657, L41.
[43]Ueta, T., Ladjal, D., & HerPlaNS Team (2012). Astronomical Society of the Pacific Conference Series 464, 59.
[44]Volk, K., & Kwok, S. (1985). A&A, 153, 79.
[45]Yu, Y. S., Nordon, R., Kastner, J. H., et al. (2009). ApJ 690, 440.
[46]Zhekov, S. A., & Perinotto, M. (1996). A&A 309, 648.

Project Scientist's Report

Martin Weisskopf

In its 14th year of operation, *Chandra* continues to facilitate outstanding science. *Chandra*'s ongoing success was validated in the most recent (2012) Senior Review of Operating Missions in Astrophysics, which rated *Chandra* highly in all categories. In particular, the Senior Review stated, "Both of these missions [*Chandra* and *Hubble*] continue to have the ability to make landmark scientific discoveries for many classes of astronomical objects. These are the two most important missions in this Senior Review." For the full report, visit http://science.nasa.gov/astrophysics/2012-senior-review/

A major highlight this past year was the first set of observations under the new proposal category "X-ray Visionary Projects (XVPs)", to address key astrophysical questions that require 1-6 Ms observing time. During this past year, evolution of the *Chandra* orbit allowed us to repeat this process, selecting four proposals: "The Small Magellanic Cloud - A Case Study of X-ray Populations at Low Metallicity" (1.1 Ms); "A Legacy Study of the Relativistic Shocks of PWNe" (1.3 Ms); "A *Chandra*-Planck Legacy Program for Massive Clusters of Galaxies" (1Ms); and "The COSMOS Legacy Survey" (2.8Ms). Visit the CXC's web site (http://cxc.harvard.edu/) for details of these exciting proposals. Overall, the Cycle 14 Peer Review approved 185 of 672 proposals, which had requested 126 Ms observing time, a factor of 5.1 oversubscription of the time available to be awarded. (See Belinda Wilkes' article for details.)

The current solar cycle (#24) is predicted to reach maximum during 2013. Thus far in this solar cycle, *Chandra* has stopped science runs 14 times through autonomous shutdowns based upon onboard measurements of hard protons, or through manual shutdowns based upon monitoring real-time measurements of soft protons by NASA's Advanced Composition Explorer (ACE). As the soft (weakly penetrating) protons damage the ACIS front-illuminated CCDs, real-time ACE data, distributed by NOAA's Space Weather Prediction Center (SWPC), are important to radiation protection of the CCDs. Although ACE is expected to operate for several more years, NOAA plans to discontinue acquisition and distribution of ACE real-time data in 2015, after the Deep Space Climate Observatory (DSCOVR) becomes operational. Consequently, Project Science is leading an assessment of the potential impact upon *Chandra* of the loss of real-time ACE data and an exploration of alternatives, to ensure we keep *Chandra* observing safely and efficiently for years to come.

Project Manager's Report

Roger Brissenden

Chandra marked over thirteen years of successful mission operations with continued excellent operational and scientific performance. Telescope time remained in high demand, with significant oversubscription in the Cycle 14 peer review, held in June. The Cycle 14 review approved 185 proposals, out of 672 submitted by researchers worldwide who requested 123 Msec of observing time, ~5.2 times greater than the time available. Among the approved proposals are four X-ray Visionary Projects (XVPs), which were allocated a total of 6 Msec. XVPs are longer observing programs intended to address major questions in astrophysics and to produce data sets of lasting value.

In the Fall, the observing program transitioned from Cycle 13 to Cycle 14. Due to the gradual evolution of *Chandra*'s orbit, which has reduced the nonproductive time spent in Earth's radiation belts, *Chandra*'s overall observing efficiency has risen to the highest level of the mission. As a result, observing Cycles 13-15 have benefited from a significant increase in available observing time. We released the Call for Proposals for Cycle 15 in December, and look forward to the Cycle 15 peer review in June 2013.

In response to NASA's request for proposals for the 2012 Senior Review of operating missions, the *Chandra* X-ray Center (CXC) submitted its proposal in January, prepared by CXC and Marshall Space Flight Center program staff, and made a presentation to the Senior Review committee in February. The committee's report rated the *Chandra* X-ray Observatory highly and described *Chandra* as one of the "two most important missions in this Senior Review." The committee recommended continuing *Chandra* operations through 2016 and augmenting the budget to make up for cuts that had been planned in the General Observer grants program.

In July, NASA extended the activities of the *Chandra* X-ray Center through September 2016 by exercising the first of two contract options. (The second option, which comes into play in 2015, would extend activities through September 2019.)

In July the CXC conducted the workshop "X-ray Binaries, 50 Years Since the Discovery of Sco X-1," and in October hosted the annual symposium for the Einstein Fellowship program. As part of the CXC's regular reviews and consultations with outside organizations, NASA reviewed the CXC's operations in April and September, and the *Chandra* Users' Committee met at the CXC in October.

After several years of very low solar radiation, the sun has become more active, requiring the team to interrupt *Chandra* observing 10 times during the year to protect the instruments from solar particles. In addition, two requests to observe targets of opportunity required the mission planning and flight teams to interrupt and revise on-board command loads. *Chandra* passed through the 2012 spring and fall eclipse seasons with nominal power and thermal performance.

In May, *Chandra* experienced a benign safemode, one of very few throughout the mission, that was caused by a small change in the performance of the active Fine Sun Sensor (FSS) near the edge of its field of view. Recovery from the safemode was smooth and rapid, aided significantly by a new command load capability that was implemented in December, 2011. We have mitigated future occurrences of the FSS effect by assuming a slightly reduced field of view, and have begun studying data from the backup FSS to assess its performance.

Chandra's focal plane instruments, the Advanced CCD Imaging Spectrometer and the High Resolution Camera, have continued to operate well and have had no significant problems. ACIS, along with the

overall spacecraft, has continued to warm gradually. All systems at the *Chandra* Operations Control Center continued to perform well in supporting flight operations. *Chandra* data processing proceeded smoothly and data distribution continued to be rapid, with the time from observation to receipt by the observer averaging ~30 hours.

In addition to producing software to support *Chandra* users with Cycle 14 observation proposal submissions, the Cycle 14 Peer Review, and the Cycle 15 Call for Proposals, the CXC's Data System team has been engaged in two major efforts: migrating the *Chandra* Data System's data processing software from Solaris to 64-bit Linux, and developing algorithms and software that will substantially increase the number of sources in the *Chandra* Source Catalog. The new catalog will incorporate fainter objects by combining multiple observations and by using new algorithms to detect on-axis sources as faint as ~5 counts, thus increasing the number of cataloged sources by a factor of ~2.5, and will for the first time include moderately extended sources. Production of the new catalog is expected to begin in late 2013.

The CXC Education and Public Outreach (EPO) group created 15 science press releases, 2 non-science press releases and 19 image releases, and produced 28 60-second High Definition podcasts on astrophysics and *Chandra* results. Two of the group's animated videos earned gold Pixie awards from the American Pixel Academy. Members of the EPO group contributed articles featuring *Chandra* science to the Spring, 2012, edition of "The Earth Scientist", a magazine for middle school teachers of Earth science and astronomy.

The EPO team presented 24 workshops at conferences and clinics sponsored by the National Science Teacher Association, the National Science Olympiad, and the American Association of Physics Teachers. EPO and CXC staff took part in the USA Science & Engineering Festival; Astronomy Night on the National Mall; a science festival in Manchester, New Hampshire, for children of National Guard troops; and events in New York City, Los Angeles and Kennedy Space Center marking the retirement of the Space Shuttle. The EPO group launched "Here, There and Everywhere", a science exhibit designed for small libraries and museums; the exhibit "From Earth to the Solar System" in conjunction with NASA's planetary division; and "STOP for Science", an informal science education program for elementary schools. In addition, the group produced training videos for users of "STOP for Science", and to support Science Olympiad Coaches' clinics.

We look forward to a new year of continued smooth operations and exciting science results.

ACIS Update

Paul Plucinsky, Royce Buehler, Nancy Adams-Wolk, & Gregg Germain

The ACIS instrument continued to perform well over the past year with no anomalies or unexpected degradations. The charge-transfer inefficiency (CTI) of the FI and BI CCDs is increasing at the expected rate. The contamination layer continues to accumulate on the ACIS optical-blocking filter. Data since April 2008, when the ACIS Detector Housing (DH) heater was turned off, indicate that the contaminant is increasing faster than previously predicted, especially along the edges of the filter. The CXC calibration group released an updated contaminant model in the CALDB 4.4.10 on 30 May 2012 to account for the increased rate of buildup. More recent data might indicate that the rate of buildup is leveling off, but more calibration observations in the future will be necessary to verify the trend.

The control of the ACIS focal plane (FP) temperature remains a major focus of the ACIS Operations Team. As the *Chandra* thermal environment continues to evolve over the mission, some of the components in the Science Instrument Module (SIM) close to ACIS have been reaching higher temperatures, making it more difficult to maintain the desired operating temperature of -119.7 C at the focal plane. In previous years, the ACIS (DH) heater and a heater on the SIM were turned off to provide more margin for the ACIS FP temperature. At this point in the mission, there are two effects that produce excursions in the FP temperature, both related to the attitude of the satellite. First, the Earth can be in the field of view (FOV) of the ACIS radiator (which provides cooling for the FP and DH). Second, for pitch angles larger than 130 degrees, the Sun illuminates the shade for the ACIS radiator and the rear surfaces of the SIM surrounding the ACIS DH. Starting in Cycle 14, the fraction of the time that the satellite spends at pitch angles more than 130 degrees should decrease as other spacecraft constraints

are relaxed; this should result in fewer excursions in the FP temperature.

Observers can help keep the FP temperature cold and stable for their observation by reducing the number of operational CCDs, which reduces the power dissipation in the FP, thereby resulting in a lower FP temperature. Starting in Cycle 13, observers were encouraged to request 5 CCDs for their observations to keep the FP and the electronics cooler, if their science objectives could be met with 5 CCDs. Starting in Cycle 14, observers were not allowed to specify "Y" for 6 CCDs in the RPS forms when they submit their proposal. If an observer requires 6 CCDs for their observation, they are to specify 5 CCDs as "Y" and one CCD as "OPT1" at the time of proposal submission. If the proposal is selected, the observer may work with their User Uplink Support Scientist and change the "OPT1" to a "Y" if the sixth CCD is required. Observers should be aware that requesting 6 CCDs increases the likelihood of a warm FP temperature and/or may increase the complexity of scheduling the observation. Observers should review the updated material in the Proposers' Guide on selecting CCDs for their observations and on this web page: http://cxc.cfa.harvard.edu/acis/optional_CCDs/optional_CCDs.html

The control of the ACIS electronics temperatures has also been a concern for the ACIS Operations Team. ACIS has three main electronics boxes, the Power Supply and Mechanisms Controller (PSMC), the Digital Processing Assembly (DPA), and the Detector Electronics Assembly (DEA). The PSMC reaches its highest temperatures when the satellite is in a "forward Sun" configuration, pitch angles between 45-60 degrees (*Chandra* cannot point within 45 degrees of the Sun). Since 2006, the *Chandra* Flight Operations Team (FOT) has been using the information provided by observers to turn off optional CCDs if thermal conditions require. As a result of the changing thermal environment, the DEA and DPA are reaching higher temperatures in tail-Sun orientations (pitch angles larger than 130 degrees). The recommendation in the previous paragraph to use only 5 CCDs if the science objectives can be met with 5 CCDs, will also reduce the temperature of the DEA and DPA in addition to the temperature of the FP. Starting in Cycle 14, the *Chandra* FOT has been using the optional CCDs information to turn off optional CCDs if either the DEA or DPA approach their temperature limits.

The ACIS flight SW team developed a patch to detect sudden increases in the count rates on all active CCDs as a means of detecting high radiation. This patch was developed in response to continued degradation in the performance of the primary radiation monitor on-board *Chandra* (EPHIN) due to increasing operational temperatures. The SW patch was uplinked to ACIS in November 2011. In May 2012, the SW for the spacecraft computer was patched to monitor the high radiation signal from ACIS and take appropriate safing actions in the case of high radiation. The combination of the ACIS radiation monitor and the HRC anti-coincidence signal will replace some of the capability lost due to a degraded EPHIN.

Important Dates for *Chandra*

Cycle 15 Peer Review: June 18-21, 2013

Cycle 14 Cost Proposals Due: Fall 2013

Users' Committee Meeting: October, 2013

Einstein Fellows Symposium: Fall 2013

Cycle 14 Start: December, 2013

Cycle 16 Call for Proposals: December, 2013

The High Resolution Camera

Ralph Kraft, Mike Juda, and Randall Smith

It has been another quiet, routine year for HRC operations. The instrument continues to perform well with no anomalies or instrumental problems. The high voltage on the HRC-S was permanently increased during the past year to recover instrument gain that was lost due to charge extraction. The loss of gain was affecting the quantum efficiency of the MCPs unevenly, affecting the observer's ability to remove the instrumental response from spectra. The on-going work to calibrate the effect of the increase in operating high voltage is discussed in the LETGS section of this newsletter. The HRC-S is now run at this higher voltage as part of routine operation, and the lower setting is no

longer used.

Two HRC-I observations of AR Lac (ObsIDs 1385 and 13182) have been used to study the system PSF at high count rates. The source flux varied during both of these observations and it was noticed that the PSF was broader during intervals of higher flux. In addition, observations of Capella, which produces a higher count rate than AR Lac, exhibited a broader PSF than AR Lac. During ground calibration at the XRCF data were taken to probe the linearity of the HRC count rate with flux, which also exhibited a broadening in the PSF with source rate. One analysis of those data compared the linearity of the core of the PSF with a surrounding annulus, showing that the rate in the core deviated from linearity at lower flux than the annulus. These measurements suggest that the increasing width of the PSF at higher count rates is due to a suppression of the peak in the core of the nominal PSF. The cascade down the channels of the MCP from an event extracts ~10^7 electrons from a very localized region. The glass in the plates has a high resistivity and the current flow required to replenish the charge lost to the event will take a finite time. Thus, it is expected that the channels will not produce the nominal response if a second event comes too soon after the first. This is an effect of event pile-up.

We can gauge the time-scale that it takes to replenish the local charge using the AR Lac and Capella observations, looking for changes in the size of the PSF as the time between successive events is decreased. Figure 1 plots the radius that encircles 85% of the source events, for events in bins of selected time since the previous source event, for three different observations. The data points in all three observations overlap and show the same trend in increasing radius as the time between events decreases. Roughly speaking, a second event in the local region arriving within 0.05s of a previous event will have been impacted by the prior event.

More details on the effect can be found at http://cxc.harvard.edu/contrib/juda/memos/hrc_pileup/index.html This web-page includes a link to a simple script that can be used to flag events that are affected proximity to a previous event in the same neighborhood, along with instructions for how to filter-out the affected events.

The HRC has been used in a wide variety of scientific measurements over the past year. In this article, we present results from an HRC-I observation of the dust-scattering halo of an X-ray binary in the Small Magellanic Cloud (SMC). Due both to its proximity and low metal abundances, the SMC provides a unique laboratory for studying the influence of metallicity and star formation on dust evolution in interstellar media beyond the Milky Way. Multiple studies have shown that the dust in the SMC is strikingly different from that in the Milky Way or even the Large Magellanic Cloud, with properties more similar to those in starburst galaxies.

This dust can be measured via the X-ray halo it creates around a bright point source, such as HMXB SMC X-1. The halo will be weak and concentrated within 30 arcsec of the source, making the HRC-I the only choice as it has the required high spatial resolution while avoiding pileup. The expected total column density was ~3×10^{21}cm^{-2}, one-third of which is Galactic. The remainder should either be local to SMC X-1 (which would not create a halo) or in the SMC itself.

Surprisingly, however, a 77 ksec observation (PI: Randall Smith) showed no significant halo from SMC dust at all, although as expected ~10^{21} cm^{-2} of Galactic dust was detected. At most 5×10^{19}cm^{-2} of SMC dust was detected, 40× less than expected. The best fit

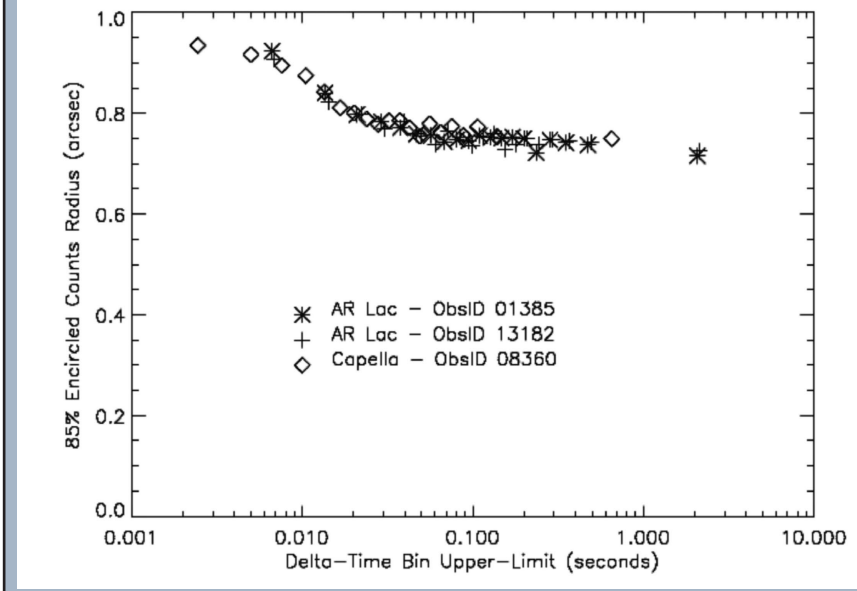

Fig. 1 - Radius in arcsec that encircles 85% of the source events, for events in bins of selected time since the previous source event, for two observations of AR Lac and one of Capella.

value (shown in red) includes a PSF and background determined from a simultaneous fit to an HRC-I observation of 3C273, which had similar count rates and so should show a similar PSF. Although there is some excess in the observation from 30–60 arcsec, the 10–30 arcsec region that should be dominated by SMC-scattered dust (purple curve) shows no sign of any halo. This could be understood if SMC X-1's absorption is entirely local to the source and there is almost no foreground SMC dust. Alternatively, the SMC dust properties in this region would have to be quite different from the Weingartner & Draine (2001) SMC "bar" dust used in this calculation, although this SMC dust model is already significantly changed from standard Galactic dust models. More work on this is in progress to determine which alternative is more likely.

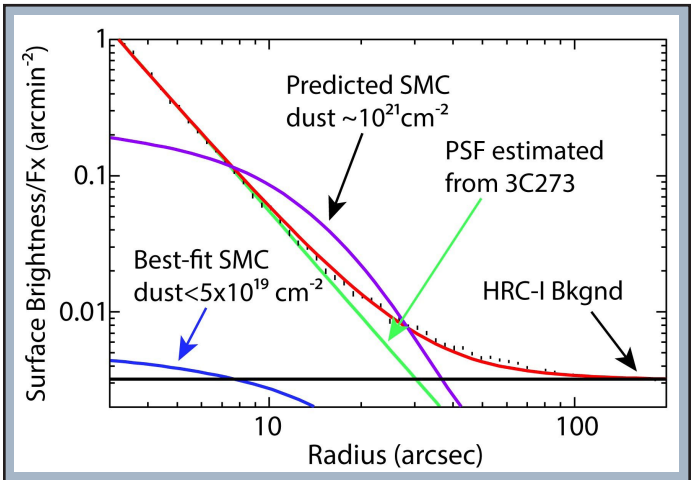

Fig. 2 - Surface brightness of dust at different SMC radii.

HETG

Dan Dewey, for the HETG Team

The HETG continues to perform as expected with no HETG-specific calibration changes made since the HETG efficiencies were updated in Dec 2011 (Marshall 2012). The main calibration change in the past year affecting the HETG was the update of the ACIS optical-blocking filter contamination model to version N0007 (in May 2012, included in CALDBs 4.4.10 and later). This updated calibration applies mainly to observations made in/after 2010; the largest flux corrections (up to 25%) are below 1 keV.

A new data analysis tool for use with HETG data has been added to CIAO 4.5: `tg_findzo`, see the `ahelp` link in the references below. This tool determines the zeroth-order centroid with sub-pixel accuracy by making use of the readout-streak events; `tg_findzo` is particularly useful for bright sources where pileup may distort the zeroth-order image causing `tg_detect` to produce an inaccurate centroid.

In terms of modeling observed spectra, Beiersdorfer et al. (2012) show some impressive progress in combining atomic theory, laboratory measurement, and HETG astrophysical data. Their new calculations of the line wavelengths emitted by Fe XVI (Na-like Fe, i.e., having a single outer M-shell electron) very nicely explain residual emission seen in the very deep HETG Capella data that have been accumulated by *Chandra*, Fig. 1.

HETG Science: Motion at the Limits

The HETG's ability to measure Doppler velocities as low as 30 km s^{-1} has been put to good use over the course of the mission. Two examples from the past year involve orbital binary motion; both push the data to their statistical limits.

The system studied by Hussain et al. (2012) consists of two M-dwarfs of 0.6 $M_{\odot}$ each in a 0.81 day orbit and having velocities of about 120 km s^{-1}. Optical observations show eclipses and determine the orbital parameters. Two HETG observations that each lasted for a full orbit, ~ 70 ks were made. The X-ray data show both flaring and quiescent emission. By extracting well-isolated emission lines and combining them in velocity space, they produce a composite line profile. This is done in a sliding time window to produce an image in velocity-time space (Figure 2). The identification of a flare to a specific binary component can be made based on the known component velocities and the observed velocity shift. The quiescent emission can likewise be studied by removing the flare times and by using only lines with low formation temperatures.

The mass ratio of objects in a binary can be determined if the orbital velocities of each component can be measured. For black holes it is hard to measure their orbital velocity, not only because they are black, but also because the emission from their accretion disks is dominated by continuum so that line measurements are generally not feasible. However Zhang et al. (2012) point out that accretion-disk winds can produce visible absorption lines in the spectrum and that

these lines (with many caveats) should have the black hole's orbital motion imprinted on them. As a "proof of concept" they have analyzed HETG observations of the binary GRO J1655-40, which consists of a ~5 $M_\odot$ black hole in a 2.6 day orbit with a ~2 $M_\odot$ companion star. Their analysis of dozens of narrow absoption lines includes a wind velocity for each line as well as the amplitude of the black hole's orbital motion, determined to be 90 km s^{-1} (Figure 3). Given the limted orbital coverage of the current data, it is certainly intriguing to see what data at other phases would show.

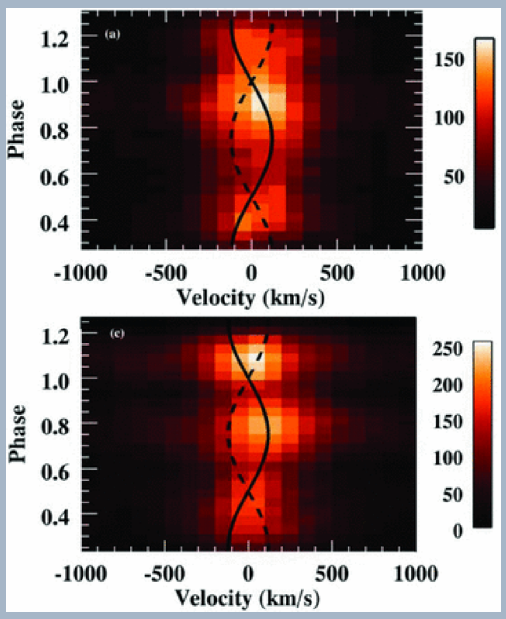

Fig.2 - Doppler images of the M dwarf binary, YY Gem. Two HETG observations each spanning a complete orbit are show with time increasing from the bottom to top, in units of the orbital phase of the system. A given horizonal row shows the observed composite velocity profile at that time. The superposed sine curves indicate the velocities of the primary (black) and secondary (dashed). The emission is dominated by three flares, seen centered near phase 0.9 in the top image and phases 0.8 and 1.1 in the bottom. The velocity profiles suggest that two of these flares (top at 0.9 and bottom at 0.8) were associated with the primary star. (From Hussain et al. 2012.)

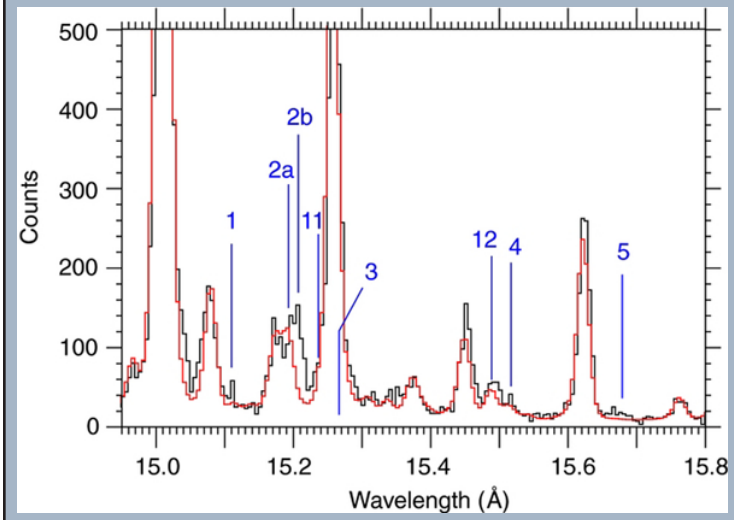

Fig.1 - Capella HETG spectra with Fe XVI lines. The HETG data (black) are reasonably fit with an APEC model (red). However, some excess emission is seen and is very well explained by the newly-calculated locations of Fe XVI L-shell lines (numbered line identifications). (From Beiersdorfer et al. 2012.)

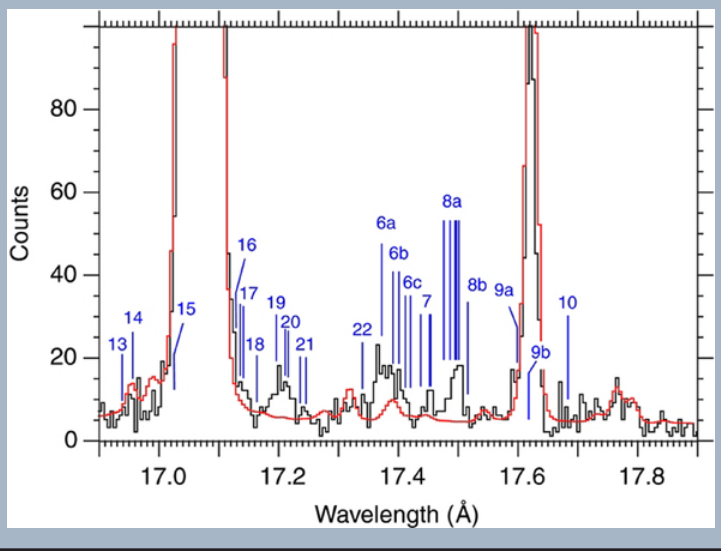

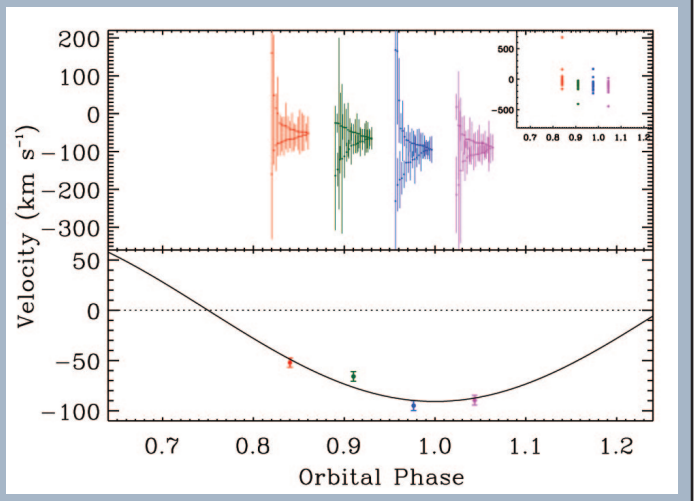

Fig.3 - Inferred orbital velocity versus orbital phase of the black-hole binary GRO J1655-40. The top panel shows the 39 individual line measurements at each of the 4 phases. The bottom panel shows the weighted average of these velocities and the best-fit orbital velocity curve (black). (From Zhang et al. 2012.)

LETG

Jeremy J. Drake for the LETG Team

High Tension

It is well-known that the working environment of the CXC is just like that of the relaxed innovation fermenters *Google* and other trendy tech megacommerce (what, time for table tennis *again*—no wonder this article is late). The title above must then refer back to *Chandra Newsletter 19*, where I described the secular gain droop experienced since launch by the HRC-S, the primary readout detector for the LETGS. Charge liberated by the ping-ponging electron cascades initiated within the microchannel pores by photon and particle interaction with the top plate of the two-plate sandwich, and amplified by 1800 V or so of high-tension, ages the plates. This occurs primarily through chemical migration in the bottom plate where the charge mainly comes from, sapping some of the instrument's photoelectric efficiency at an average rate of about 0.6% per year. It is a known behavior of microchannel plates and can in principle be remedied by increasing the high tension to compensate. In the same *Newsletter 19*, HRC instrument scientist Ralph Kraft described the procedure we adopted to investigate the voltage change required to recover the gain—basically making stepwise adjustments of the voltage during real-time telemetry contact in the middle of an observation of the LETG standard candle HZ43, hoping the instrument did not get upset, all while playing table tennis.

The experiment worked: the gain was observed to increase in a linear, well-behaved fashion with increases in voltage in 20V steps across top and bottom plates. Comparison of the mean detector pulse height amplitude for the HZ43 photon events dispersed over the outer plates of the detector for the different voltages with those observed earlier in the mission enabled us to determine the voltage settings needed to restore the initial on-orbit performance. The gain change with voltage seen in the real-time telemetry passes are illustrated in Figure 1, showing the analysis by Brad Wargelin made during occasional breaks between sets. Settings for the blue curve were chosen for the new operating voltage. These corresponded to potential differences of 1819.6 V across the bottom plate and 1791.0 V across the top.

One of the problems we hoped to remedy by restoring the gain was the steady decline in the detector quantum efficiency that has accompanied the gain droop (see *Newsletter 19*). The QE could be re-calibrated using further observations of HZ43 obtained at the new adopted voltage settings, at least for wavelengths down to 50 Å or so. At shorter wavelengths, things get a bit more tricky, since we run out of point-like steady sources of cosmic X-rays and have to rely on ones that vary. Observations of the blazar Mkn 421 were therefore planned for last July, at both new and old voltages, relying on the source not to vary too much during the observations so that we could discern the voltage-related count rate differences. The source behaved for the first half of the observation, then bolted off toward higher fluxes nearer the end. The voltage changes were, however, cunningly interleaved with LETG+ACIS-S observations to provide a comparison, and we were still able to determine the higher energy QE change to a precision of about 1.5%.

Expert *Chandra* analyst Nick Durham reduced and blended all the data together into a thick, creamy sauce, and after the ping-pong balls settled we found that the raised voltage saw a jump in the QE by about 6% at the longest wavelengths and lowest energies, with the change declining in magnitude going toward higher energies by a percent or two. This trend is not unexpected: the gain droop caused a small fraction of the lowest pulse height photon events to be lost to the particle background noise and an event lower level threshold discriminator. Since the mean pulse height increases with increasing photon energy, the largest QE loss, and conversely the largest QE recovery, is then expected for the lower energy photon events.

The QE is actually a three-dimensional function—of the two spatial dimensions of the detector as well as photon energy—and we have only re-calibrated it essentially in one dimension. This calibration is then only valid if the QE changed by the same amount over the whole detector. Indications are that this is a pretty good assumption, but perhaps not quite good enough, with potential changes in the QE uniformity of the order of a few percent. Calibrating the QEU on the ground is relatively straightforward—the detector can be placed in front of a uniformly-illuminating X-ray source. In-flight, we have the worst case scenario: focusing of the uniformly-illuminating X-ray source to a single point by the most precise X-ray mirrors ever made. Getting around this stunning design defect will present considerable difficulties for us in the coming year. . . oh, already time for another game?

Broadening Horizons

If there is a celestial source designed by nature for application of a slitless, high-resolution X-ray spectrometer, it is the massive stellar wind. Spatially point-like, there are no overlapping dispersed images to disentangle, as is the case for significantly extended sources. The wind is thought shocked to X-ray temperatures, either by line-driven acceleration instabilities, or by the aid of magnetic channeling, and emits discrete spectral lines that can provide diagnostics of temperature, density and the strength of the local UV radiation field. On top of this, wind terminal velocities often exceed 1000 km s^{-1}—sufficiently large that they can be resolved by *Chandra*'s gratings to truly utilize the dispersion, or velocity, dimension. Two recent papers have exploited LETGS spectra to tackle outstanding problems in high-mass stellar winds.

One is the "weak wind" problem, first identified from UV and optical spectra and described as "urgent" in the review of Puls et al (2008). The problem arises in the later-type O and early B dwarfs. Ultraviolet line profiles clearly show classical P Cygni wind signatures, but modeled mass-loss rates can be an order of magnitude lower than theoretical expectations. This is important because mass loss from hot stars can be sufficient to influence the evolution of the star itself and tends to dominate the injection of mass and energy into the ambient interstellar medium, playing a key role in cosmic feedback.

The ultraviolet, of course, does not tell the whole

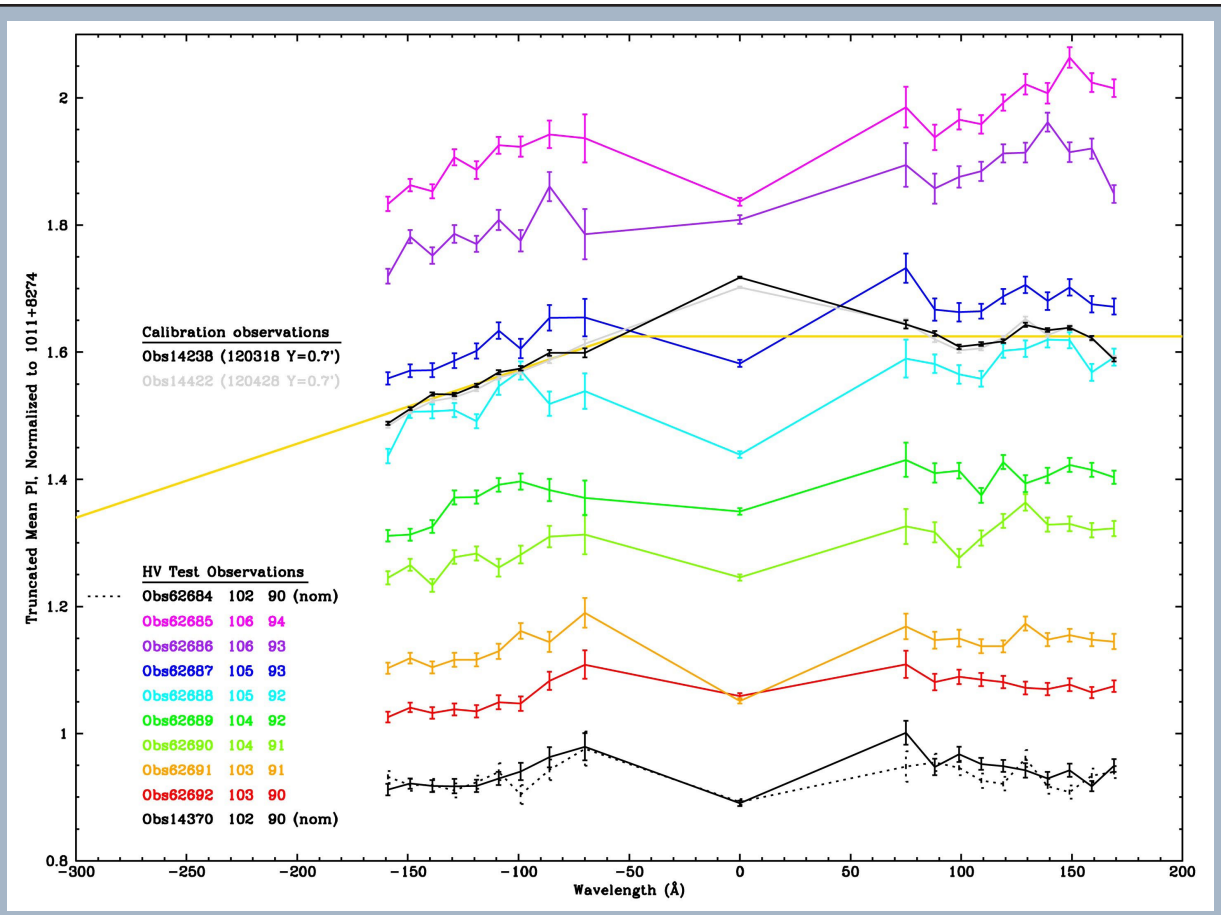

Fig. 1.— The mean pulse heights for 0th order and slices of dispersed HZ43 spectra, using the old gain calibration, and normalized to data obtained at the "old" voltage settings (ObsIDs 1011 and 8274). Colored curves and the bottom two black curves (solid and dotted) are for short test observations at various voltage settings. The different settings are denoted by a voltage "step" number for top and bottom plates listed after each ObsID. Settings for the blue curve (ObsID 62687) were chosen for the new operating voltage. The upper black and gray curves are for 10 ks calibration observations made with the new voltages. (0th order appears high for these two observations because they were made with Y-offset=0.7', which moves 0th order off a low-gain "burned-in" region at the on-axis aimpoint.) The gold line segments represent the gain correction factor used for pulse height-based background filtering in post-voltage-change observations.

story. Since shock-heating to X-ray temperatures is expected, and in analogy with other searches for missing baryons, the natural place to look for any hidden mass is in the X-ray spectral region. Huenemoerder et al. (2012) observed the prototypical weak-wind O star μ Columbae using the LETG and ACIS-S, together with Suzaku. Line profiles like that of O VIII illustrated in Figure 2 betray the hot, high-velocity wind, with a terminal velocity of 1600 km s^{-1}. Even the small blueshift in the line profile expected because of some obscuration of the redshifted hemisphere by the central star might be discernible, though is not formally detected. The X-ray emission measure indicated that the outflow is almost an order of magnitude greater than that derived from UV lines and is consistent with the canonical wind–luminosity relationship for O stars. The wind is hidden from UV scrutiny because it is too hot and ionized. Huenemoerder et al. (2012) conclude that the "weak-wind" problem is largely, and perhaps completely, resolved by accounting for the hot wind seen in X-rays but not in the UV.

The very nature of the shocked-wind paradigm for single O-stars was questioned by Pollock (2007) based on *XMM-Newton* observations of the O9.7 Ib supergiant component of the ζ Orionis system. The X-ray spectrum lacked evidence of substantial variation with wavelength of either plasma emission measure or velocity width that was expected in the instability-driven shock model. Pollock also noted that the spectrum appeared largely optically thin, and suggested that X-rays are not from the dense, central regions of the wind where it is strongly accelerated, but from further out in the terminal velocity region. The shocks would then be collisionless and might explain another problem with the canonical model: that otherwise fairly similar O stars exhibit a scatter of an order of magnitude in X-ray luminosity. Magnetic fields in the region where the shocks occurred could then be the "missing variable" accounting for the scatter. Other essentially single O stars could provide further tests of the hypothesis.

Raassen and Pollock (2013) use the LETG+HRC-S to observe the O9.5 supergiant δ Orionis. Particular attention was paid to the He-like ions to establish the distance of the X-ray emitting ions from the stellar surface based on the UV excitation of the intercombination lines. The spectrum appeared thermal, and consistent with collisional equilibrium. The X-ray emitting plasma was found to be located 2–80R_* from the stellar surface based on lines of Mg XI to C V, with

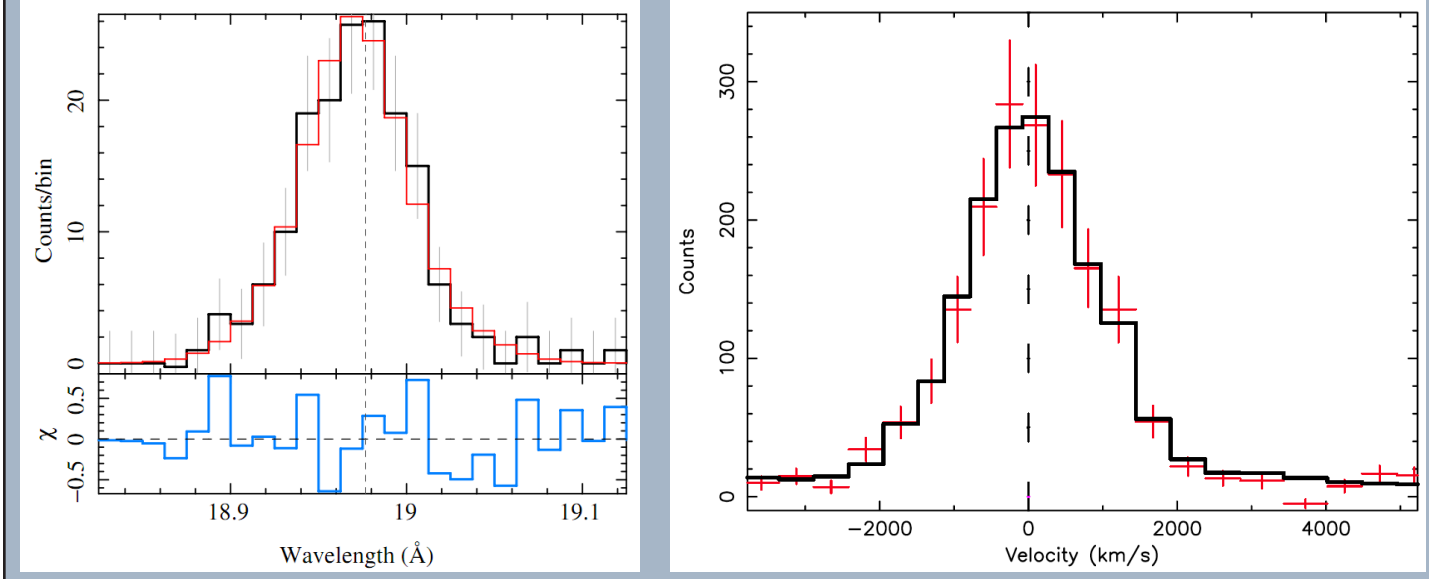

Fig. 2.— Velocity-broadened profiles of the H-like O VIII λ18.97 Lyα line providing key diagnostics for O star winds. Left: The O VIII profile (black) seen in the LETG+ACIS-S spectrum of the O 9.5V "weak-wind" star μ Col. A wind model with terminal velocity $v\infty$ = 1600 km s^{-1} is shown in red, together with residuals in lower panel. The wind model indicates that nearly all the wind mass is at X-ray temperatures, eluding detection in the UV and alleviating the weak wind problem. From Huenemoerder et al. (2012). Right: The profile of the O VIII line in the LETG+HRC-S spectrum of the O9.5 supergiant δ Ori that tests the collisionless shock scenario of Pollock (2007). Observations are illustrated in red, together with a fitted Gaussian model in black (note that the instrumental line spread function is also significant here). The rest wavelength is also shown. The HWHM of ~840 km s^{-1} is possibly too small for a uniform, spherically-symmetric shocked-wind, and might betray the presence of self-obscuring clumps. From Rassssen and Pollock (2013).

the cooler ions located farther out in the wind, similar to the case of ζ Ori. Lines from the hot ions Mg XI, Ne IX, and O VIII, were formed close-in, however—from 2 to 10R_*. The latter data then tend to support the canonical model, with shocks formed near the acceleration region of the deeper, more dense wind, rather than much farther out. This raises the possibility that both shock regimes are present.

Even such a mixed shock scenario is not quite that simple of course. Raassen and Pollock suggest that line profiles with HWHM ~840 km s^{-1} are narrower than would be expected based on a wind terminal velocity of 2000 km s^{-1}. The observed O VIII line profile is shown in Figure 2. One possible explanation is that shocked clumps in the wind are self-shielding, with X-ray emission then preferentially observed orthogonally to the wind velocity vector, toward the limb where the line-of-sight velocity is small.

More observations, or at least a couple of games of table tennis, are clearly needed.

JJD thanks Ralph Kraft, Mike Juda, Brad Wargelin and the LETG team for useful comments, information and discussion.

References

[1]Raassen, A. J. J. & Pollock, A. M. T. (2013). A&Ap 550, A55.
[2]Huenemoerder, D. P., Oskinova, L. M., Ignace, R., Waldron, W. L., Todt, H. , Hamaguchi, K., Kitamoto, S. (2012). ApJL 756, L34.
[3]Puls, J., Vink, J, & Najarro, F. (2008). A&ApR 16, 209-325.
[4]Pollock, A. M. T. (2007). A&Ap 463, 1111-1123.

Updates to *Chandra* Calibration in 2012

Larry David

Nine updates to the *Chandra* calibration database (CALDB) were released during 2012. The CALDB releases contained the standard quarterly calibration updates of the ACIS-S and ACIS-I gain tables and the yearly calibration updates of the HRC-I gain table. The increase in the operating high voltage of the HRC-S in April, 2012 necessitated the release of two gain tables for the HRC-S (one for the old high voltage setting and one for the new high voltage setting).

During the past year, a revised ACIS contamination model and a set of time-dependent ACIS QE maps were released. Both of these calibration products affect the effective area of ACIS. An analysis of ACIS external calibration source (ECS) data acquired during the *Chandra* mission shows that the QE has declined since launch by about 5% on the BI chips and by 3% on the FI chips. To correct for this effect, a set of time-dependent ACIS QE maps (one for every two years) was released. CIAO tools automatically select the appropriate QE map for any observation. The ECS data, along with monitoring observations of Abell 1795, also show that the condensation rate of the molecular contaminant onto the ACIS filters increased slightly over the past few years. In addition, the spatial pattern of the contamination on the ACIS filters changed during this time. Accordingly, a new ACIS contamination model was released in May, 2012. The new contamination model mainly affects data taken since 2009. The correction to the ACIS effective area with the latest contamination model can be up to 10% at 0.5 keV for observations taken in early 2012.

While the QE of the HRC-I has been very steady, the QE of the HRC-S along the dispersion direction of LETG spectra has declined by about 5% during the *Chandra* mission. To restore the declining HRC-S QE, the operating high voltage of the HRC-S was increased in April, 2012. LETG/HRC-S calibration observations of a soft source (the white dwarf HZ43) and a hard source (the blazar Mkn421) were then taken with the new high voltage setting to re-calibrate the detector. These observations showed that the HRC-S QE with the new high voltage setting is very similar to the launch QE. Using the the HZ43 and Mkn421 observations, the CXC calibration team released new versions of the HRC-S QE and gain in 2012. The CIAO software will automatically use the appropriate calibration products when analyzing HRC-S data.

The aim-point on the focal plane detectors has drifted slightly during the course of the mission (see the POG for a more in-depth discussion). Due to this drift, the zeroth order of LETG/HRC-S spectra shifted onto a new HRC-S tap (the region between adjacent pre-amps) during parts of the dither pattern. The de-gapping procedure of the data acquired in this new tap region produced some distortion in the zeroth order image. Since the wavelength scale in dispersed spectra is computed relative to the centroid of the zeroth order image, the distortion in the zeroth order image can produce a systematic shift in the wavelength scale. The lack of good de-gap coefficients near the new HRC-S aim-point was simply due to a lack of existing data

in this region. To remedy this problem, the calibration team carried-out a LETG/HRC-S observation of HZ43 with the zeroth order image centered on the new tap, from which new de-gap coefficients were derived. Updated HRC de-gap coefficient tables were then released to the public in June, 2012 to correct the distortion in the zeroth order image.

The *Chandra* calibration team continues to support the efforts of the International Astronomical Consortium for High Energy Calibration (IACHEC). Several CXC calibration scientists attended the 7th annual IACHEC meeting in Napa, California in March, 2012. These meetings bring together calibration scientists from all present and many future X-ray and γ-ray missions. Collaborations established at these meetings have led to a number of cross-calibration papers published in the Journal of Astronomy & Astrophysics.

Chandra Related Meetings

Check our website for details:
http://cxc.harvard.edu/

Galaxy Workshop
Dates TBD
DoubleTree Guest Suites, Boston, MA
http://cxc.harvard.edu/cdo/xgals13/

Einstein Fellows Symposium
Fall 2013
http://cxc.harvard.edu/fellows/

Publishing Chandra Results

Adding Power to Your Papers through Data Linking

Arnold Rots and Sherry Winkelman

Following a suggestion by the Chandra Users' Committee, we are planning to add a README file to all data distributions from the Chandra Data Archive. This file will contain some observation-specific information, but will also provide hints on how to add power to your published papers and how to publish value-added data products through the Chandra Data Archive (CDA). The README especially draws the user's attention to the following three considerations when preparing a publication based on Chandra data: data references, high-level science data products, and acknowledgments.

In the following "`<ObsId>`" should be replaced by the actual ObsId in five-digit form (i.e., with leading zeroes).

Data References

Please include a list of the ObsIDs and/or Dataset Identifiers for the data reported in your manuscript to ensure that archive users can easily find and cite your results. The Dataset Identifier for a particular observation is: `ADS/Sa.CXO#obs/<ObsId>`

A Dataset ID can be inserted in a LaTeX manuscript using AASTeX as:
`\dataset [ADS/Sa.CXO#obs/<ObsId>] {Chandra ObsId <ObsId>}` or in any manuscript as a footnote providing the following URL: ivo://ADS/Sa.CXO#obs/`<ObsId>`.

If you include the results from a large number of observations in your article you may want to ask CDA Operations to assign a customized defined dataset identifier: http://cxc.harvard.edu/cgi-gen/cda/specreq. See also: http://cxc.harvard.edu/cda/datasetid.html

High-Level Science Data Products

The CXC is eager to have the Chandra Data Archive serve as a long-term data repository for valuable high-level data products, and to make these datasets citable in the literature. This includes the data behind any figures or tables in your published articles. See http://cxc.harvard.edu/cda/contributedsets.html

Acknowledgments

Authors of publications that use Chandra data (whether new or archived) are asked to include an acknowledgment similar to the following:

For articles by a PI team: The scientific results reported in this article are based on observations made by the Chandra X-ray Observatory.

For articles based on archival data: The scientific results reported in this article are based [if applicable: in part or to a significant degree] on data obtained from the Chandra Data Archive.

For articles based on published results: The scientific results reported in this article are based [if applicable: in part or to a significant degree] on observations made by the Chandra X-ray Observatory and published previously in cited articles.

Or any combination of these. Please include a grant number if the research was supported by a Chandra Award. See also the current guidelines for Chandra Science Publications at: http://cxc.cfa.harvard.edu/cdo/scipubs.htmlChandra Data Archive Operations (arcops@head.cfa.harvard.edu)

CIAO 4.5

Improved tools and Sherpa, ability to merge observations and now featured on YouTube!

Antonella Fruscione, for the CIAO Team

Version 4.5 of CIAO and CALDB 4.5.5, the newest versions of the *Chandra* Interactive Analysis of Observations software and the *Chandra* Calibration Database, were released in December 2012. CIAO 4.5 (cxc.harvard.edu/ciao) includes numerous enhancements and bug fixes with respect to previous CIAO versions, all listed in detail in the software release notes. We will describe here some of the most notable changes and improvements.

CIAO Tools

• The new `tg_findzo` tool helps users locate the source position for grating data with a piled or blocked zero order.

In general the `tgdetect` tool is used to find the centroid of the zero-order image in a grating event list. If the zero-order source is piled-up, there is the potential for the centroid to be incorrect due to the "hole" created in the data. Also, when observing a bright source, an observer may choose to have the zero-order region blocked via on-board software to avoid telemetry problems. The new tool is useful in determining the correct source position for a grating observation with either a piled or blocked zero order. New spectral data is extracted with the updated source position. `tg_findzo` works by computing the intersection of the data dispersed along one of the grating arms and the readout streak that is associated with bright sources.

•Various updates were added related to creating merged datasets, especially larger mosaics that exceed the standard image sizes. This includes updates to `reproject_events` and `dmmerge` to adjust the limits based on the data and to `dmextract` to keep a consistent definition of BACKSCAL regardless of image size.

•the `modelflux` tool has a new option to calculate the unabsorbed flux. If the user does choose this new option, then both absorbed and unabsorbed fluxes are calculated and reported to the screen in addition to being written to the `modelflux` parameter file. Users are reminded that the `mkpsf` tool is now retired and either ChaRT (cxc.harvard.edu/chart/) or MARX (http://space.mit.edu/cxc/marx-4.5/) should be used to simulate the *Chandra* point spread function. We are actively working to make these tools easier to use in the global CIAO context.

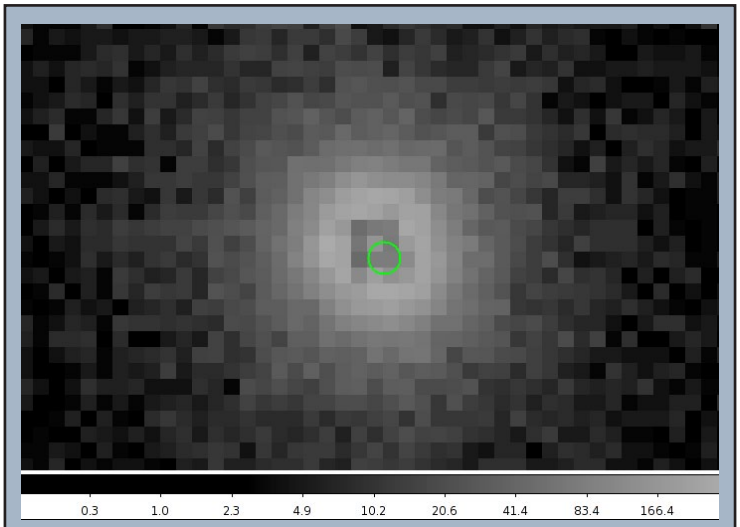

Figure 1: The zeroth order location determined by `tgdetect`. The image has been zoomed in and the region radii reduced to show that the zeroth order location is offset from the true center of the source, which will cause wavelength shifts in the extracted spectrum. Using the zeroth order location will cause systematic errors in the wavelengths and may lead to invalid results.

Figure 2: The zeroth order location determined by `tg_findzo`. The image has been zoomed in and the region radii reduced to show the zeroth order. The solid green circle is the new `tg_findzo` result compared to the incorrect `tgdetect` location (yellow, dashed).

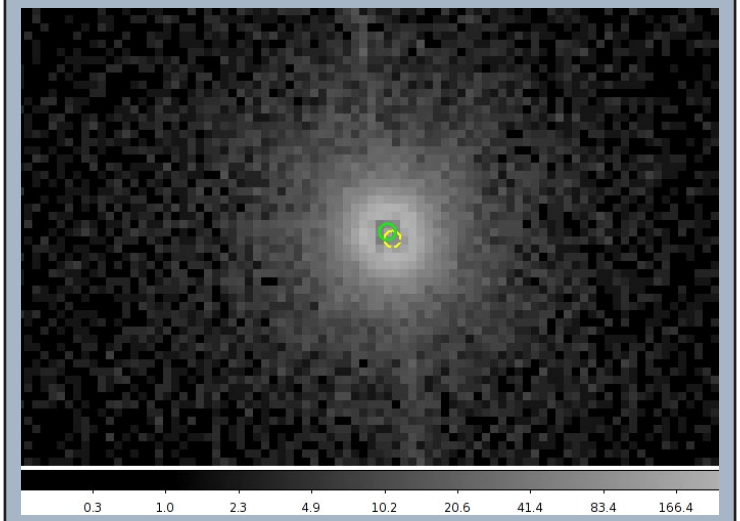

CIAO Scripts

The CIAO contributed scripts package (cxc.harvard.edu/ciao/download/scripts/) is considered a required part of the software installation and contains analysis scripts and modules written by scientists at the CXC. These scripts and modules automate repetitive tasks and extend the functionality of the CIAO software package by filling specific analysis needs. The package is updated about once a month and concurrently with major CIAO releases. For CIAO 4.5, all scripts were retested to ensure that they run smoothly within the new system.

A few weeks before the CIAO release, the new scripts `merge_obs`, `reproject_obs`, and `flux_obs` were released together with much improved version of the `fluximage` script and extensive documentation on how to use them. These scripts (which globally replace the "old" `merge_all` script which is now deprecated) are designed to easily reproject and merge observations, with the option of creating exposure-corrected images of the combined data. `Fluximage` creates exposure-corrected images and exposure maps for ACIS or HRC observation.

ChIPS

ChIPS (cxc.harvard.edu/chips/) is the imaging and plotting platform for CIAO which can be used during data analysis — to plot a lightcurve or a spectrum — and to create publication-quality figures. ChIPS is designed for use in a variety of modes: as a user-interactive application and in batch mode. ChIPS is an importable module for the Python scripting language and is available as a C/C++ library for software developers.

In the CIAO 4.5 release of ChIPS the major update is the support for adding annotations (labels, lines, regions, and color bars) directly from the ChIPS GUI; other changes include improvements and fixes to both the GUI and a range of commands.

A large gallery of ChIPS examples is included in the ChIPS website at cxc.harvard.edu/chips/gallery/ and there are a number of introductory threads to guide beginners.

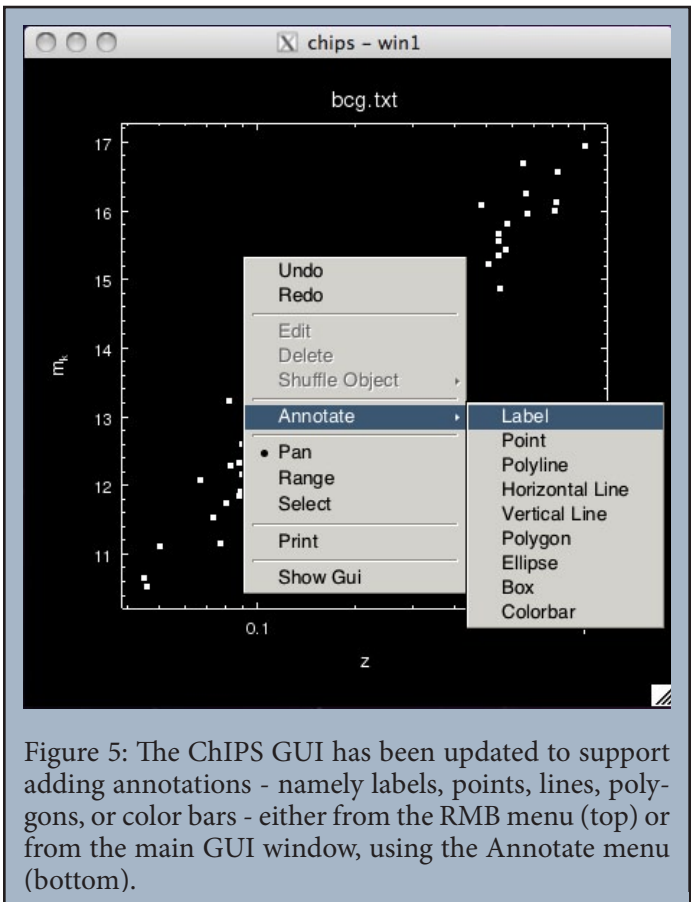

Figure 5: The ChIPS GUI has been updated to support adding annotations - namely labels, points, lines, polygons, or color bars - either from the RMB menu (top) or from the main GUI window, using the Annotate menu (bottom).

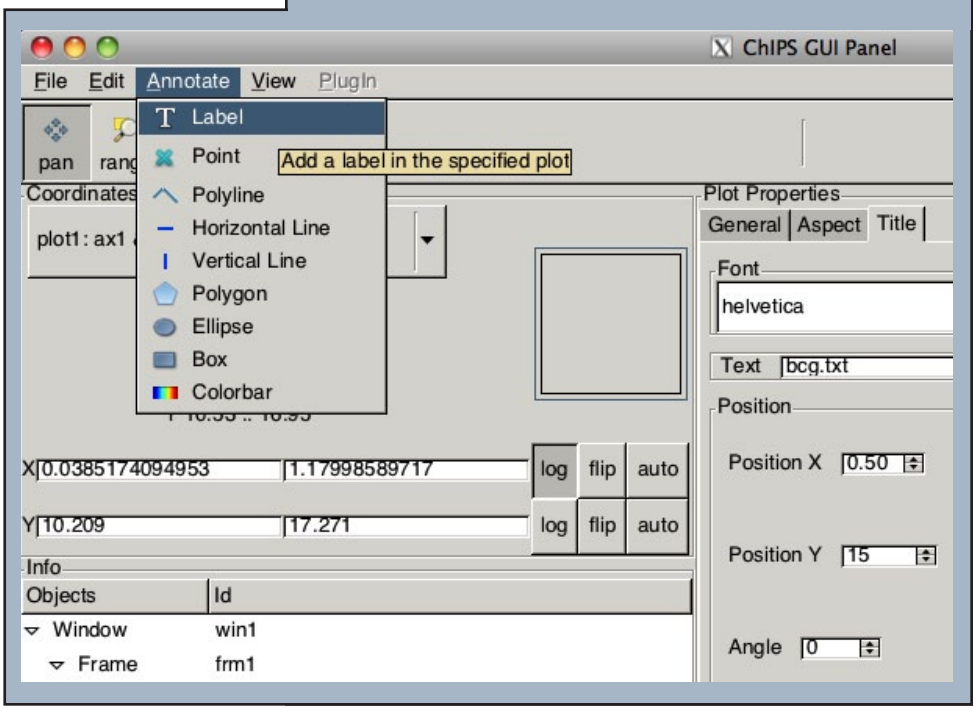

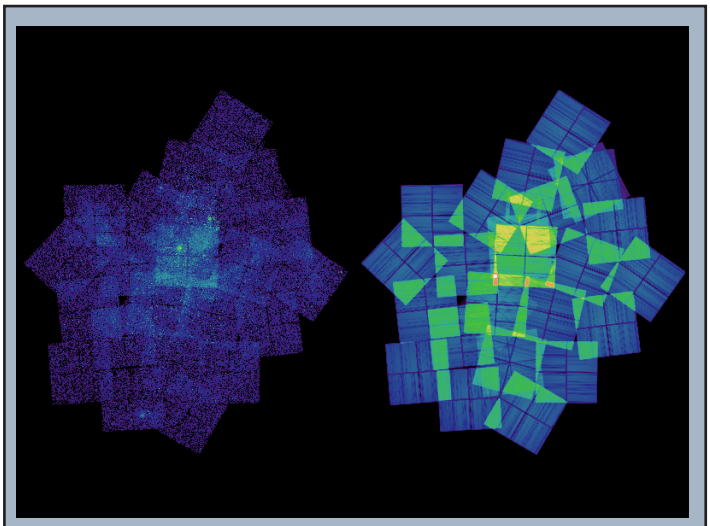

Fig. 3: The left image shows the broad (0.5 to 7.0 keV) band data for the neighborhood around Eta Carinae, and the right image shows the exposure map for this data set, calculated assuming a monochromatic source emitting at 2.3 keV. The data consists of 41 ACIS-I observations, downloaded using `find_chandra_obsid`, processed with `chandra_repro`, and aligned and combined using `merge_obs` (the S-array chips were excluded in this analysis). The output image has 1363 x 1537 pixels, with a pixel size of 3.936 arcseconds (8 times the default ACIS pixel scale).

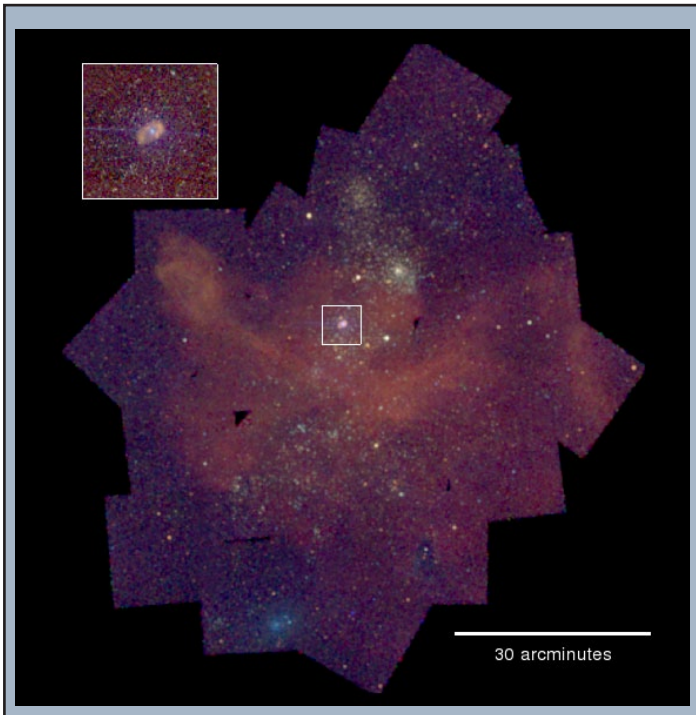

How Did We Combine the Data?

A) What data is available?

The *Chandra* Footprint Service at http://cxc.harvard.edu/cda/footprint/ allows you to search for observations that overlap a position. We can use the `find_chandra_obsid` script to perform this search from the command line, including some basic filtering options:

% `find_chandra_obsid` 'eta carinae'
% `find_chandra_obsid` 'eta carinae' radius=60
% `find_chandra_obsid` 'eta carinae' inst=acisi radius=60

B) Download the data

Now we have decided on the observations we are interested in, we can download them from the archive:

% `find_chandra_obsid` 'eta carinae' inst=acisi radius=60 download=all

A simple way to list the obsids we have downloaded is to change the detail level:

% `find_chandra_obsid` 'eta carinae' inst=acisi radius=60 detail=obsid > obsids.lis

C) Reprocess the data

A recent change to the `chandra_repro` script lets us reprocess all the observations with just one call; it will however take some time for this particular example!

% `chandra_repro` indir=@obsids.lis outdir=.

D) Create the combined, exposure-corrected, images

% `merge_obs` "*/repro/*evt2.fits[ccd_id=0:3]" combined/ bands=broad,csc

Note that we use the ccd_id filter to get only the near-axis ACIS-I FI chips. This will eventually create the exposure-corrected images combined/<band>_flux.img, where <band> is one of soft, medium, hard and broad.

Fig. 4: A three-color image - visualized with ChIPS - of the Eta Carinae nebula, using the 0.5 to 1.2 keV, 1.2 to 2.0 keV, and 2.0 to 7.0 keV pass bands for the red, green, and blue channels respectively. Each band was divided by its corresponding exposure map (evaluated at 0.92, 1.56, and 3.8 keV) before being combined. The image size and pixel scale is the same as the previous figure, but it has been smoothed by a Gaussian with a sigma of 12 arcseconds, and a log scale applied, to bring out the diffuse emission. The inset shows a zoom in of the Eta Carinae nebula with no smoothing. The almost-horizontal blue line is the read-out streak from the central object.

Sherpa

Sherpa (cxc.harvard.edu/sherpa/) is the modeling and fitting application within CIAO and can be used for analysis of images, spectra and time series from many telescopes, including optical telescopes such as *Hubble*. Sherpa is flexible, modular and extensible. It has an IPython user interface and it is also an importable Python module. Sherpa models, optimization and statistical functions are available via both C++ and Python for software developers wishing to link such functions directly to their own compiled code. Important changes and additions to the Sherpa functionality in the CIAO 4.5 release are described in a dedicated webpage at cxc.harvard.edu/sherpa/updates.html Among several improvements to the software, we highlight two features:

`sample_flux`: this new function has been added to calculate the energy flux with uncertainties due to a Sherpa model. It returns a sample of parameters with a corresponding flux and a flux uncertainty for a model component or a combination of model components. The model components have to be previously defined and used in the fit. The samples are generated from the multi-variate normal distributions with the scales defined by covariance (if at the best fit) or supplied (as "scales"). The flux is calculated for each set of new parameters. The returned flux value is given by a sample's median with the lower and upper quantiles defined by the confidence level supplied to the function.

Modeling of non X-ray data: a set of optical models (e.g. `absorptionedge`, `emissionlorentz`, etc.) is now available allowing users to model emission and absorption lines in optical spectra. Also XSPEC models such as for example `xsdiskbb`, or `xsdiskpn` work in Sherpa with ASCII-type data and do not require any response files; this makes the models easily useable for optical-UV data from non X-ray observatories.

CIAO on YouTube

Since interactive or graphical features, like the interaction of CIAO with the `ds9` imager, can be difficult to describe in a static document, we have attempted to capture this experience on a YouTube channel. The "4ciaodemos" channel at http://www.youtube.com/user/4ciaodemos features tutorials, demos, and screen-casts of CIAO. It currently contains 13 videos which already have 1060 views and counting. Sit back, relax and watch CIAO in action! More information and updates on CIAO can always be found at http://cxc.harvard.edu/ciao/ or subscribe to the CIAO News RSS feed at cxc.harvard.edu/ciao/feed.xml To keep up-to-date with CIAO news and developments, subscribe to chandra-users@head.cfa.harvard.edu Just send e-mail to 'majordomo@head.cfa.harvard.edu', and put 'subscribe chandra-users' (without the quotation marks) in the body of the message.

Useful *Chandra* Web Addresses

To Change Your Mailing Address:
http://cxc.harvard.edu/cdo/udb/userdat.html

CXC:
http://chandra.harvard.edu/

CXC Science Support:
http://cxc.harvard.edu/

CXC Education and Outreach:
http://chandra.harvard.edu/pub.html

Science Publication Guidelines
http://cxc.harvard.edu/cdo/scipubs.html

ACIS: Penn State
http://www.astro.psu.edu/xray/axaf/

High Resolution Camera:
http://hea-www.harvard.edu/HRC/HomePage.html

HETG: MIT
http://space.mit.edu/HETG/

LETG: MPE
http://www.mpe.mpg.de/xray/wave/axaf/index.php

LETG: SRON
http://www.sron.nl/divisions/hea/chandra/

CIAO:
http://cxc.harvard.edu/ciao/

Chandra Calibration:
http://cxc.harvard.edu/cal/

MARX simulator
http://space.mit.edu/ASC/MARX/

MSFC: Project Science:
http://wwwastro.msfc.nasa.gov/xray/axafps.html

The Results of the Cycle 14 Peer Review

Belinda Wilkes

The observations approved for *Chandra*'s 14th observing cycle are now in full swing and the Cycle 15 Call for Proposals (CfP) was released on 13 December 2012. Cycle 13 observations are nearly complete.

The Cycle 14 observing and research program was selected as usual, following the recommendations of the peer review panels. The peer review was held 25–29 June 2012 at the Hilton Boston Logan Airport, a week later than usual due to the lateness of the summer AAS meeting. More than 100 reviewers from all over the world attended the review, sitting on 15 panels to discuss 672 submitted proposals (Figure 1). The Target Lists and Schedules area of our website provides lists of the various types of approved programs, including abstracts. The peer review panel organization is shown in Table 1.

The Cycle 14 CfP included a second call for X-ray Visionary Projects (XVPs). XVPs are major, coherent science programs to address key, high-impact scientific questions incurrent astrophysics that require 1-6 Ms of observing time. As in Cycle 13, the evolution of *Chandra*'s orbit results in a larger amount of available observing time as a lower fraction of each orbit is spent within the radiation belts. This allowed observing time to be allocated to XVPs without impacting the time available for GO proposals and Large Projects (LPs). The total amount of time allocated in Cycle 14 was 23.3 Ms, including 6.2 Ms awarded to 4 XVPs and 5.7 Ms to 12 LPs. The response to the XVP opportunity continued to be very positive. The oversubscriptions in telescope time for LPs and XVPs were 6.6 and 6.7 respectively. The overall oversubscription in observing time was 5.3 (Figure 2), typical of the past few cycles despite the much larger amount of time being allocated (Figure 3). The continued evolution of the *Chandra* orbit has allowed us to include a smaller (5 Ms) XVP program in the Cycle 15 CfP.

Table 1: Panel Organization

Topical Panels:	
Galactic	
Panels 1,2	Normal Stars, WD, Planetary Systems and Misc
Panels 3,4	SN, SNR + Isolated NS
Panels 5,6,7	WD Binaries + CVs, BH and NS Binaries, Galaxies: Populations
Extragalactic	
Panels 8,9,10	Galaxies: Diffuse Emission, Clusters of Galaxies
Panels 11,12,13	AGN, Extragalactic Surveys
XVP Panel	X-ray Visionary Proposals
Big Project Panel	LP and XVP Proposals

Following our standard procedure, all proposals were reviewed and graded by the topical panels, based primarily upon their scientific merit, across all proposal types. Each topical panel received an initial allocation of *Chandra* time for GO observing propos-

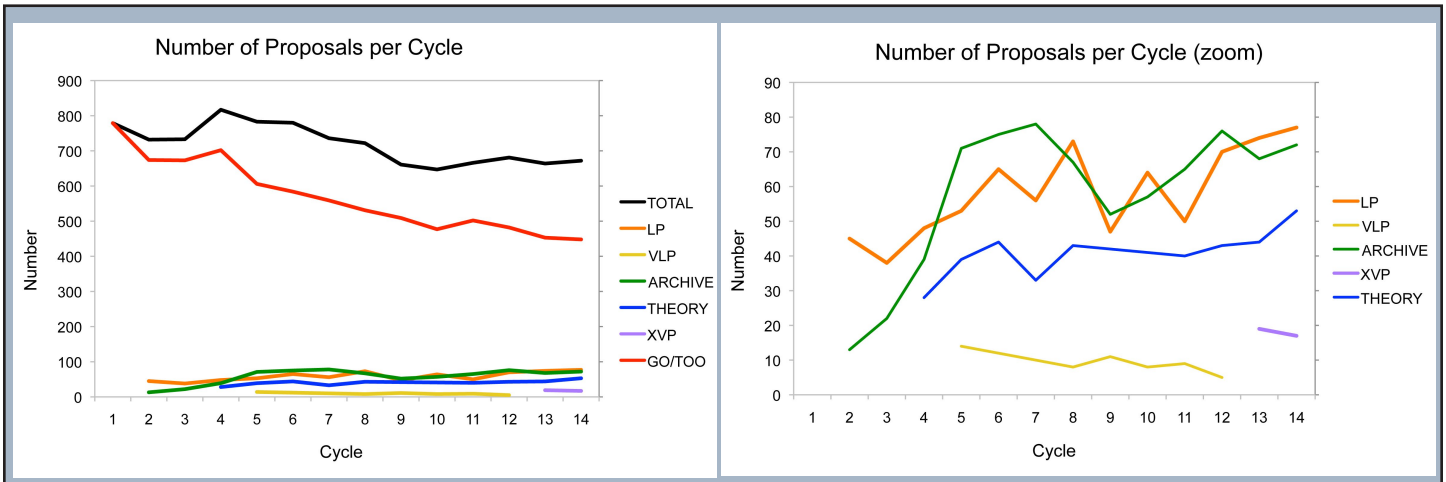

Fig. 1 - a: The number of proposals submitted in each proposal category (e.g. GO, LP, Archive etc.) as a function of cycle., b: zoom on lower curves. Since more proposal types have become available in each cycle, the number classified as GO has decreased as other types increase. The total number of submitted proposals has remarkably constant over the past 7-8 cycles.

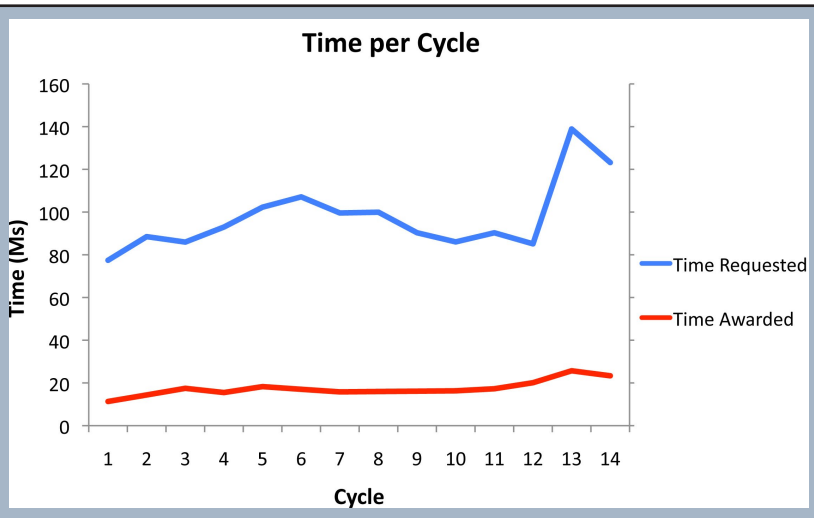

Fig. 2 - The requested and approved time in Msec as a function of cycle, including allowance for the probability of triggering each TOO. This increased somewhat over the first few cycles, the largest effect being due to the introduction of Very Large Projects (VLPs) in Cycle 5. The subsequent increase in requested and awarded time in Cycles 13 and 14 is clear.

als based upon the demand for time in that panel. Other allocations to each panel included: joint time, TOOs with a < 30 day response, time constrained observations in each of 3 classes, time in future cycles and money to fund archive and theory proposals. These were based on the full peer review oversubscription ratio. The topical panels produced a rank-ordered list along with detailed recommendations for individual proposals where relevant. A report was drafted for each proposal by one/two members of a panel and reviewed by the deputy panel chair before being delivered to the CXC. Panel allocations were modified, either in real time during the review or after its completion, to transfer unused allocations between panels so as to follow the panel recommendations as far as possible.

LPs and XVPs were discussed by the topical panels and ranked along with the GO, archive and theory proposals. In addition, the XVPs were discussed and ranked by a separate XVP/pundit panel. The topical and XVP panels' recommendations were recorded and passed to the Big Project Panel (BPP), which included all topical panel chairs and members of the XVP panel. The schedule for the BPP at the review included time for reading and for meeting with appropriate panel members to allow coordination for each subject area. The BPP discussed the LPs and XVPs separately and generated two rank-ordered lists. The meeting extended into Friday afternoon to allow for additional discussion and a consensus on the final rank-ordered lists to be reached. A small amount of observing time was transferred between the two lists during these final deliberations to ensure that all observing time was allocated. BPP panelists updated review reports, both at the review and remotely over the following 2 weeks, to include the BPP discussion.

The resulting observing and research program for Cycle 14 was posted on the CXC website on 20 July 2012, following detailed checks by CXC staff and approval by the Selection Official (CXC Director). All peer review reports were reviewed by CXC staff for clarity and consistency with the recommended target list. Formal e-letters informing the PIs of the results, providing budget information (when appropriate) and providing a report from the peer review, were e-mailed to each PI in early August.

Joint Time Allocation

Chandra time was also allocated to several joint programs by the proposal review processes of *XMM-Newton* (2 proposals) and HST (3 proposals).

The *Chandra* review accepted joint proposals with time allocated on: *Hubble* (12), *XMM-Newton* (2), NRAO (14), and NOAO (3).

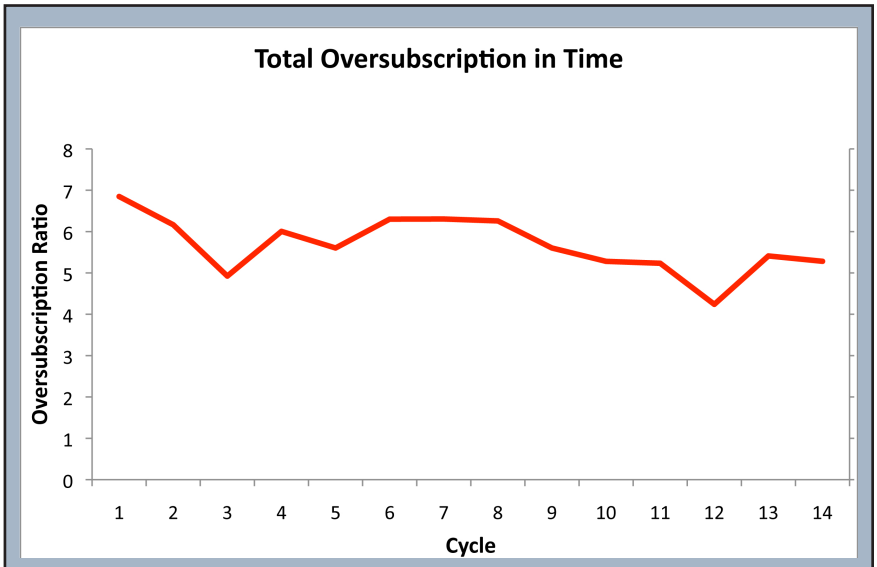

Fig. 3 - The final oversubscription in observing time based on requested and allocated time in each cycle. Again the numbers are remarkably constant. The decrease in Cycle 12 reflects the late 16% increase in the amount of time awarded by the peer review in that cycle to offset the significantly increasing observing efficiency as the orbit evolved (see article in 2011 Newsletter).

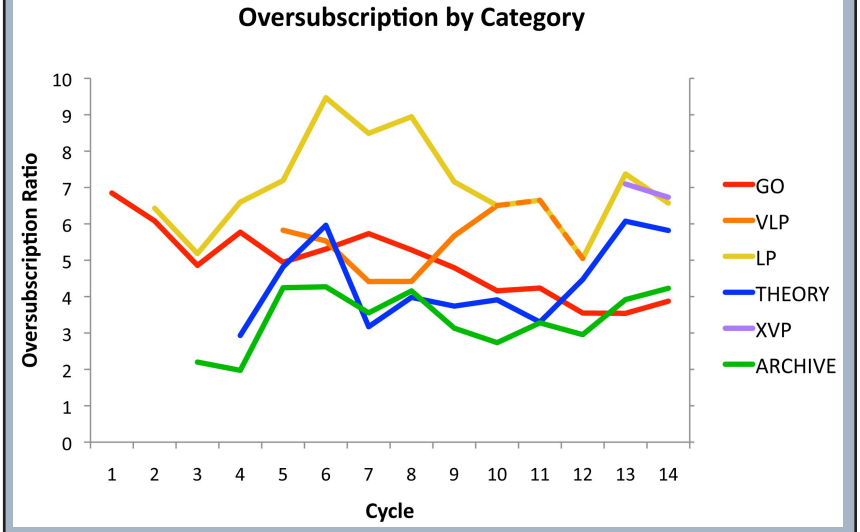

Fig. 4 - The effective oversubscription ratio in terms of observing time for each proposal category as a function of cycle. Oversubscription for Archive and Theory categories is shown by funding. Please note that some of the fluctuations are due to small number statistics (e.g. Theory proposals).

Constrained Observations

As observers are aware, the biggest challenge to efficient scheduling of *Chandra* observations is in regulating the temperature of the various satellite components (see POG Section 3.3.3). In Cycle 9 we instituted a classification scheme for constrained observations which accounts for the difficulty of scheduling a given observation (CfP Section 5.2.8). Each class was allocated an annual quota based on our experience in previous cycles. The same classification scheme was used in Cycles 10-14. In Cycles 13 and 14 the quotas were increased commensurate with the larger amount of observing time to be awarded. There was a large demand for constrained time so that not all proposals which requested time-constrained observations and had a passing rank (>3.5) could be approved. Effort was made to ensure that the limited number of constrained observations were allocated to the proposals ranked highest, review-wide. Detailed discussions were carried out with panel chairs to record the priorities of their panels in the event that more constrained observations could be allocated. Any uncertainty concerning priorities encountered during the final decision process was discussed with the relevant panel chairs before the recommended target list was finalized.

Please note that the most over-subscribed constraint class was: "EASY" while "AVERAGE" was only marginally over-subscribed. In practice, these two classes were combined when determining which observations should be allocated time. The same 3 classes will be retained in Cycle 15 so as to ensure a broad distribu*tion in the requested contraints. We urge proposers to specify their constraints as needed by the science.*

Cost Proposals

PIs of proposals with US collaborators were invited to submit a Cost Proposal, due in Sept 2012 at SAO. In Cycle 14 each project was allocated a budget based on the details of the observing program (see CfP Section 8.4). Awards were made at the allocated or requested budget levels, whichever was lower. The award letters were emailed in late November, in good time for the official start of Cycle 14 on 1 Jan 2013.

Proposal Statistics

Statistics on the results of the peer review can be found on our website: under "Target Lists and Schedules:" select the "Statistics" link for a given cycle. We present a subset of those statistics here. Figure 4 displays the effective oversubscription rate for each proposal type as a function of cycle. Figures 5, 6 show the percentage of time allocated to each science category and to each instrument combination. Table 2 lists

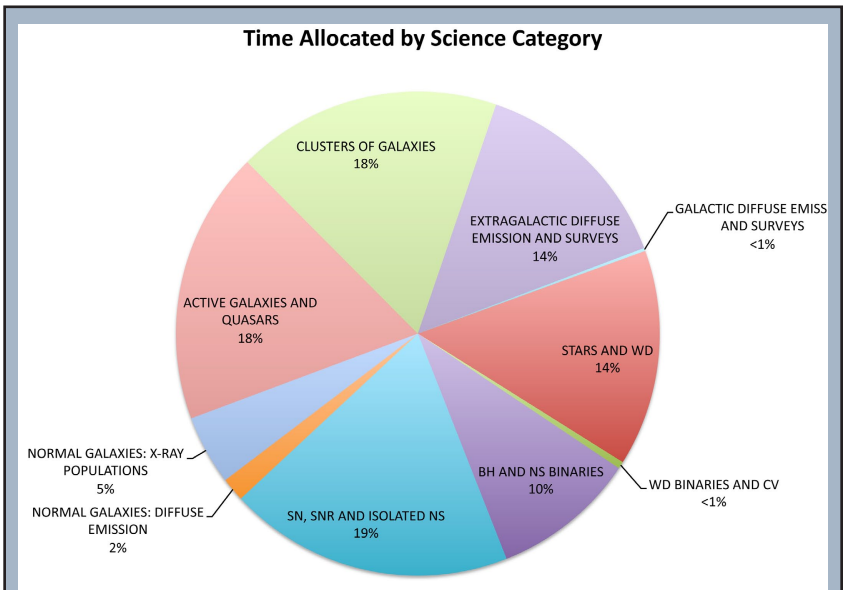

Figure 5: A pie chart indicating the percentage of *Chandra* time allocated in each science category. Note that the time available for each category is determined by the demand.

the numbers of proposals submitted and approved, per country of origin.

Table 2: Number of Requested and Approved Proposals by Country

Country	Requested		Approved	
	# Proposals	Time (ksec)	# Proposals	Time (ksec)
USA	512	94577.7	151	21097.8
Foreign	160	31378.2	34	3714.00
Country	Requested		Approved	
	# Proposals	Time (ksec)	# Proposals	Time (ksec)
Argentina		90.00		
Australia	4	795.00		
Austria	1	30.00	1	30.00
Belgium	3	1010.00		
Bulgaria	2	205.00		
Canada	14	1748.00	5	330.00
Chile	1	283.00		
China	1	50.00		
Finland	1	22.00		
France	4	2360.00	2	180.00
Germany	33	8289.00	3	306.00
India	6	555.00		
Ireland	2	35.00		
Israel	2	325.00		
Italy	22	4124.00	5	722.00
Japan	6	679.00	2	145.00
Korea	1	198.10		
Mexico	1	170.00	1	170.00
Netherlands	10	1037.00	4	431.00
Russia	1	105.00		
Spain	9	611.00	2	115.00
Switzerland	1	30.00		
Taiwan	2	307.00		
Turkey	4	397.00		
U.K.	28	7923.10	9	1285.00

* Note: Numbers quoted here do not allow for the probability of triggering TOOs

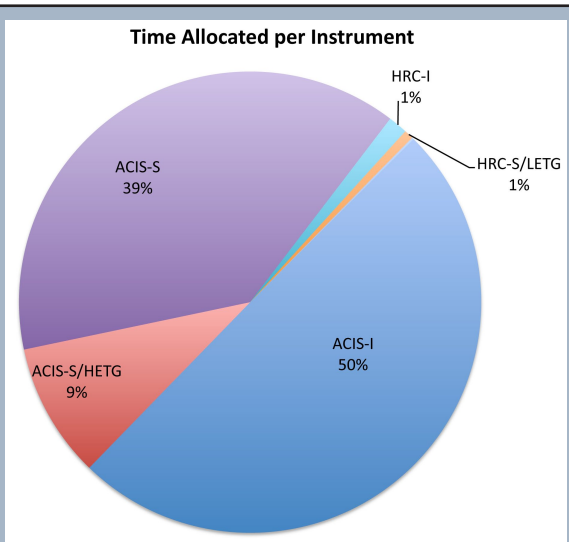

Figure 6 : A pie chart showing the percentage of *Chandra* time allocated to observations for each instrument configuration.

Einstein Postdoctoral Fellowship Program

Andrea Prestwich

The Call for Proposals for the 2013 class of Einstein Fellows was released in July 2012. This is the 5th year of the Einstein Fellowship Program, which started in 2008 when the *Chandra* and *Fermi* Fellowship programs were combined. Interest in the program remains very high with 190 applications for 12 Fellowships. The Fellowship Selection Panel met January 15-16, and all candidates received a "sorry", "wait list" or "offer" email on the afternoon of January 16. As of this writing (January 2013) finalists are considering their offers. We expect the 2013 Fellows to be finalized by February 15.

The 2012 Fellowship Symposium was held in October here at the Harvard-Smithsonian Center for Astrophysics (CfA). The talks were terrific and much enjoyed by scientists from the CfA and other institutions in the neighborhood.

This year the application process was managed by a completely new software package (Fellowship Management Software, FMS). It was designed and coded by *Chandra* X-ray Center programmers, and is tailored explicitly to the Einstein Program. The FMS

is web-based and used for all steps in the selection process: receipt of applications, assigning reviewers to candidates, generating a shortlist of applicants to be discussed at the Selection Panel, and finalizing a rank-ordered list of winners at the Selection Panel. The FMS has worked extremely well, and will be extended over the next year or so track current Fellows activities (for example, annual reports and travel requests).

Einstein Fellows have had some notable successes this year. Matt McQuinn (2009 cohort) is currently a *Hubble* Fellow at University of California at Berkeley and will move to a faculty position at the University of Washington in 2014. Justin Vandenbroucke (2012 cohort) has been offered a faculty position at the University of Wisconsin, Madison and Phil Hopkins (2011 cohort) will take up a faculty position at Caltech in the fall of 2013. Emily Levesque (2010 cohort) was awarded the 2012 Robert J. Trumpler award from the Astronomical Society of the Pacific. Einstein Fellows have also made headlines this year! A paper by Akos Bogdan (2011 cohort) on high black-hole-to-bulge mass ratios in two early-type galaxies (Bogdan et al 2012, ApJ 753, 140B) was the subject of a press release at the American Astronomical Society meeting in Anchorage, Alaska. Sam Gralla's paper on the "Thermodynamics of a Black Hole with a Moon" (arXiv:1210.8444) was showcased by New Scientist magazine in November 2012. Rubens Reis (2011 cohort) had a press release on a QPO in a tidal disruption event (http://www.nasa.gov/mission_pages/swift/bursts/shredded-star.html). Congratulations to all Fellows on a productive year!

Chandra Users' Committee Membership List

The Users' Committee represents the larger astronomical community for the *Chandra* X-ray Center. If you have concerns about *Chandra*, contact one of the members listed below.

Name	Organization	Email
Lee Armus	SSC	lee@ipac.caltech.edu
Franz Bauer	SSI	fbauer@spacescience.org
Tiziana DiMatteo	CMU	tiziana@lemo.phys.cmu.edu
Erica Ellingson	CASA-Colorado	erica.ellingson@colorado.edu
Jimmy A. Irwin	University of Alabama	jairwin@ua.edu
Tim Kallman	GSFC	Timothy.R.Kallman@nasa.gov
Carol Lonsdale	NRAO	clonsdal@nrao.edu
Hironori Matsumoto	Nagoya University	matumoto@u.phys.nagoya-u.ac.jp
Jon Miller (Chair)	University of Michigan	jonmm@umich.edu
Rachel Osten	STScI	osten@stsci.edu
Pedro Rodriguez	ESA	prodrigu@sciops.esa.int
John Tomsick	UC Berkeley	jtomsick@ssl.berkeley.edu
Ex Officio, Non-Voting		
Lia LaPiana	NASA HQ	Lia.S.LaPiana@nasa.gov
Larry Petro	NASA HQ	Larry.D.Petro@nasa.gov
Wilt Sanders	NASA HQ	wsanders@hq.nasa.gov
Allyn Tennant	NASA/MSFC, Project Science	allyn.tennant@msfc.nasa.gov
Martin Weisskopf	NASA/MSFC	martin@smoker.msfc.nasa.gov
CXC Coordinator		
Paul Green	CXC Director's Office	pgreen@head.cfa.harvard.edu

CXC 2013 Press Releases

Megan Watzke

Date	PI	Objects	Title
10 January	Felipe Menantaeu (Rutgers)	ACT-CL J0102-4915 ("El Gordo")	NASA's *Chandra* Finds Largest Galaxy Cluster in Early Universe
8 February	Kastytis Zubovas (Univ. of Leicester)	Sgr A*	NASA's *Chandra* Finds Milky Way's Black Hole Grazing on Asteroids
21 February	Ashley King (Univ. of Michigan)	IGR J17091-3624	NASA's *Chandra* Finds Fastest Wind From Stellar-Mass Black Hole
02 April		Einstein Fellows	2012 Einstein Fellows Chosen
30 April	Roberto Soria (Curtin Univ.)	M83	NASA's *Chandra* Sees Remarkable Outburst From Old Black Hole
4 June	Francesca Civano (CfA)	CID-42	Giant Black Hole Kicked Out of Home Galaxy
11 June	Akos Bogdan (CfA)	NGC 4342 and NGC 4291	Black Hole Growth Found to be Out of Synch
15 August	Michael McDonald (MIT)	SPT-CLJ2344-4243 ("Phoenix Cluster")	Phoenix Cluster Sets Record Pace at Forming Stars
27 August	Kim Arcand (CfA)	Here, There, and Everywhere project	New Exhibit Connects Science from Here, There, and Everywhere
24 September	Anajli Gupta (Ohio State)	Milky Way Halo	NASA's *Chandra* Shows Milky Way is Surrounded by Halo of Hot Gas
28 November	Teddy Cheung (National Academy of Sciences/NRL)	GB 1428+4217	Record-Setting X-ray Jet Discovered
18 December	Julie Hlavacek-Larrondo (Stanford)	18 galaxy clusters	From Super to Ultra: Just How Big Can Black Holes Get?
Links to all of these press releases can be found at http://www.*Chandra*.harvard.edu/press/12_releases/			
Additional image releases and other features that were issued during 2012 are available at: http://www.*Chandra*.harvard.edu/photo/chronological12.html			

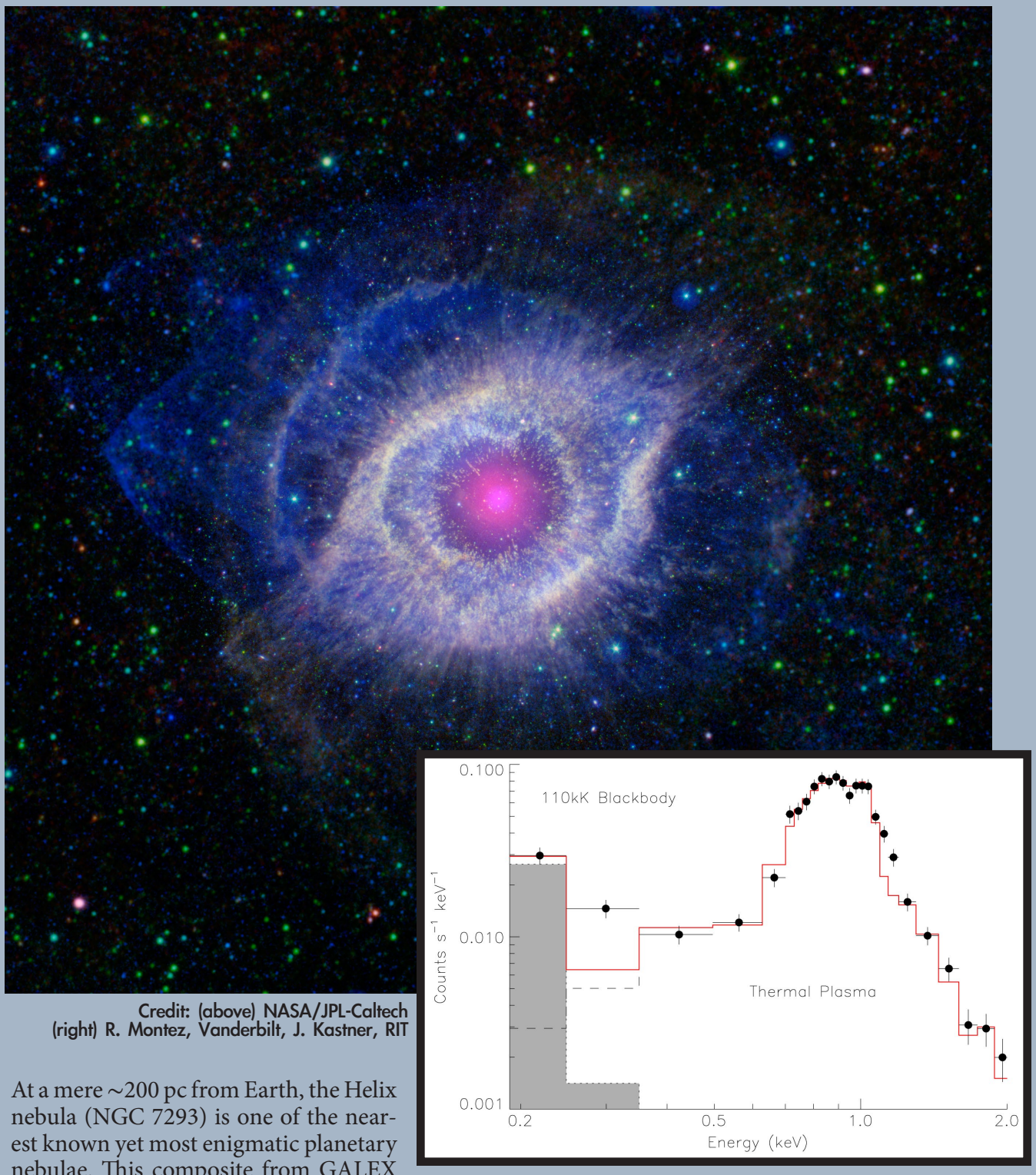

Credit: (above) NASA/JPL-Caltech
(right) R. Montez, Vanderbilt, J. Kastner, RIT

At a mere ~200 pc from Earth, the Helix nebula (NGC 7293) is one of the nearest known yet most enigmatic planetary nebulae. This composite from GALEX (UV; blue), *Spitzer*, and WISE (IR; red, yellow, and green) imagery reveals the complex structure of the extended nebula resulting from the ejection and subsequent ionization of the envelope of the progenitor AGB star. At the nebula's core, the central star retains a significant mid-IR excess (shown in red in the composite image), indicative of a residual, Kuiper-Belt-like debris disk. The Chandra spectrum of the remnant stellar core (inset) reveals an unexpectedly hard source of X-rays. Such relatively hard, point-like X-ray sources are surprisingly common within planetary nebulae, although their underlying physical mechanism(s) remains uncertain (see section 2 of cover story).